

Composite Life Cycle of West Pacific Jet-Superposition Events and the Large-Scale Environmental Response over Western North America

ZACHARY J. HANDLOS^a AND JONATHAN E. MARTIN^a

^a *Georgia Institute of Technology, Atlanta, Georgia*

(Manuscript received 11 May 2020, in final form 21 November 2020)

ABSTRACT: Vertical alignment of the polar and subtropical jet streams in the west Pacific basin occurs most often during the boreal cold season. Recent work has revealed that the large-scale environment conducive to producing such superpositions involves interaction between East Asian winter monsoon cold-surge events, lower-latitude convection, and internal jet dynamics. The evolution of the large-scale environments associated with these events post-superposition as well as the significance of that evolution on aspects of the wintertime Northern Hemisphere general circulation is examined through construction of a 44-case composite. The post-superposition west Pacific jet extends eastward associated with an anomalous positive–negative geopotential height couplet straddling the jet’s exit region. This jet extension results in ridge building over Alaska and northwestern Canada. The large-scale evolutions associated with the composite post-superposition environment occur consistently among the majority of cases considered within this analysis. The positive–negative geopotential height anomaly couplet, enhanced jet entrance circulation, low-latitude convection, and internal jet dynamics present in the pre-superposition environment weaken post-superposition. As a result, the characteristic vertical PV “wall” associated with the composite vertically superposed jet weakens. Last, investigation of the value of using the two most dominant modes of west Pacific jet variability in observing the evolution of the superposed west Pacific jet post-superposition reveals that, while the extension of the jet is exhibited, significant variability exists when analyzing each of the 44 cases of interest individually.

KEYWORDS: Jets; Synoptic-scale processes; Upper troposphere

1. Introduction

The genesis, evolution, and dissipation of extratropical weather systems and related midlatitude phenomena are often linked to the evolution of the Northern Hemisphere polar and subtropical jet streams, which have been researched extensively over the past several decades. The polar jet resides above regions of strong baroclinicity within the midlatitudes (usually poleward of 30° latitude), and its speed maxima is observed ~300 hPa. The polar jet is also referred to as the “eddy-driven” jet, with many studies demonstrating that the polar jet results from convergence of eddy momentum flux associated with developing waves in a region of enhanced midlatitude baroclinicity (e.g., Held 1975; Rhines 1975; McWilliams and Chow 1981; Panetta 1993). The subtropical jet resides primarily within the upper troposphere on the poleward edge of the Hadley cell (Krishnamurti 1961), is associated with a weaker and shallower horizontal temperature gradient than the polar jet (e.g., Defant and Taba 1957; Winters and Martin 2014) and is primarily driven by angular momentum transport via convection in the equatorial latitudes.

Both the polar and subtropical jets reside in regions of strong gradients in tropopause height and potential vorticity. This is consistent with observations (e.g., Davies and Rossa 1998) as

well as theory, which clearly relates strong gradients in quasi-geostrophic potential vorticity (QGPV) to local maxima in geostrophic wind speed (see Cunningham and Keyser 2004; Handlos and Martin 2016; Christenson et al. 2017, for a more detailed explanation). Defant and Taba (1957) were the first to note the relationship between the jets and a steep tropopause. They constructed maps of tropopause height and noted the related regions of sharp gradients in such depictions were observationally related to the two jets. The subtropical jet resides between the “tropical” and “subtropical” tropopause steps while the polar jet resides between the “subtropical” and “polar” tropopause steps. Such “steps” are clearly discernible in mean meridional cross sections (e.g., see Figs. 1a and 1b in Handlos and Martin 2016).

Substantial research exists regarding the polar and subtropical jets. Examples include early research studies focusing on the general characteristics of the jets (e.g., Namias and Clapp 1949; Defant and Taba 1957; Riehl 1962; Reiter 1963), specifically the subtropical jet stream (e.g., Loewe and Radok 1950a,b; Mohri 1953; Koteswaram and Parthasarathy 1954; Krishnamurti 1961), the role of jet streams within the general atmospheric circulation (e.g., Yeh 1950; Koteswaram 1953; Sutcliffe and Bannon 1954; Palmén and Newton 1969), their dynamical influence on the evolution of baroclinic waves and surface development (Shapiro et al. 1999), and also the role of these jet streams with respect to frontal boundaries (e.g., Newton 1954; Keyser and Shapiro 1986; Shapiro and Keyser 1990). However, considerably less research attention (until recently) has been given to instances of the vertical superposition of the polar and subtropical jets, referred to as “vertical jet-superposition events” (Winters and Martin 2014; Handlos

Martin’s current affiliation: University of Wisconsin–Madison, Madison, Wisconsin.

Corresponding author: Zachary J. Handlos, zachary.handlos@eas.gatech.edu

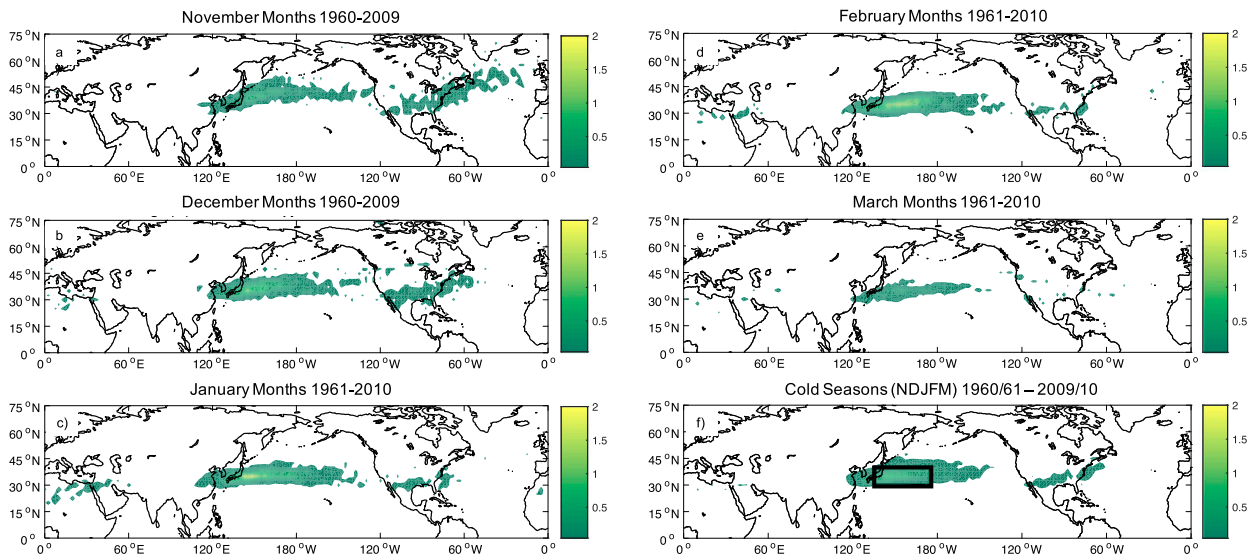


FIG. 1. Adapted from Christenson et al. (2017). (a) Percentage of 6-hourly dates/times within (a) November 1960–2009, (b) December 1960–2009, (c) January 1961–2010, (d) February 1961–2010, (e) March 1961–2010, and (f) cold-season months NDJFM 1960/61–2009/10, in which a JSID is detected at each grid point over the Northern Hemisphere. Note that (f) also includes the boxed region of interest considered in identifying “robust” west Pacific vertical jet-superposition events within this study.

and Martin 2016; Winters and Martin 2016; Christenson et al. 2017; Winters and Martin 2017; Winters et al. 2020). Vertical jet-superposition events result in a single jet core with wind speed maxima notably stronger than the separate polar and subtropical jets (see Fig. 8 of Christenson et al. 2017). Prior work has also identified the leading structural characteristic of such features to be the deep, nearly vertical tropopause “wall” separating, in one step, the tropical from the polar tropopause. Such a structure departs from the more common two steps along the tropopause staircase characteristic of environments in which the two jets are separate (see Fig. 2 and discussion in Handlos and Martin 2016).

Mohri (1953) was the only work known to the authors of this study that investigated a west Pacific vertical jet-superposition event prior to the last decade. Recently, Christenson et al. (2017) constructed a Northern Hemisphere climatology of such events, finding that the maximum frequency of occurrence of superpositions occurs during the boreal cold season (i.e., November–March) within the west Pacific. These events are uncommon. Figure 1 (reproduced from Christenson et al. 2017) shows the number of jet-superposition identifications that occur on average within each month (or cold season) referenced in each panel between boreal cold seasons during 1960/61–2009/10. The figure shows that a vertical jet-superposition event at any given grid point within the NCEP–NCAR Reanalysis 1 dataset only occurs in about 1%–2% of all 6-hourly time periods during the cold season (NDJFM) even in the regions of highest frequency of occurrence (though jet-superposition events can occur multiple times within a cold season, such as the multiple events observed within the 1995–96 boreal winter season shown in Table 1, for example).

Handlos and Martin (2016) composited 44 boreal winter west Pacific vertical jet-superposition events and investigated

the evolution of the large-scale environments conducive to polar–subtropical jet superposition (Fig. 2). They found that several key large-scale features associated with the East Asian winter monsoon are tied to west Pacific vertical jet-superposition events. The East Asian winter monsoon is driven by the Siberian–Mongolian surface high pressure system (e.g., Chan and Li 2004) which, during an East Asian winter monsoon cold

TABLE 1. List of 44 robust west Pacific vertical jet-superposition events identified using the methodology described in section 2.

Robust event time and date	Robust event time and date
0000 UTC 7 Feb 1980	1200 UTC 14 Feb 1999
0600 UTC 29 Dec 1980	0000 UTC 23 Dec 1999
0600 UTC 11 Jan 1981	0600 UTC 31 Jan 2000
1200 UTC 29 Jan 1981	1200 UTC 16 Feb 2000
1800 UTC 14 Dec 1981	0000 UTC 17 Feb 2000
1800 UTC 15 Dec 1981	0600 UTC 11 Dec 2000
0600 UTC 4 Feb 1987	0000 UTC 4 Jan 2001
0000 UTC 10 Jan 1988	1200 UTC 4 Jan 2001
1200 UTC 23 Feb 1991	0000 UTC 15 Jan 2001
1800 UTC 24 Feb 1991	1200 UTC 15 Jan 2001
1200 UTC 25 Feb 1991	0000 UTC 16 Jan 2001
1800 UTC 24 Feb 1993	1800 UTC 19 Feb 2002
0000 UTC 25 Dec 1995	0000 UTC 21 Dec 2003
1800 UTC 25 Dec 1995	1800 UTC 26 Dec 2003
0000 UTC 1 Feb 1996	0600 UTC 7 Feb 2004
1200 UTC 2 Feb 1996	1800 UTC 27 Dec 2005
0000 UTC 1 Dec 1996	0000 UTC 10 Jan 2007
1200 UTC 1 Dec 1996	0000 UTC 15 Feb 2008
0000 UTC 2 Dec 1996	0000 UTC 16 Feb 2008
1200 UTC 9 Jan 1999	1800 UTC 16 Feb 2008
1200 UTC 12 Jan 1999	1200 UTC 8 Jan 2010
0000 UTC 13 Feb 1999	1200 UTC 15 Jan 2010

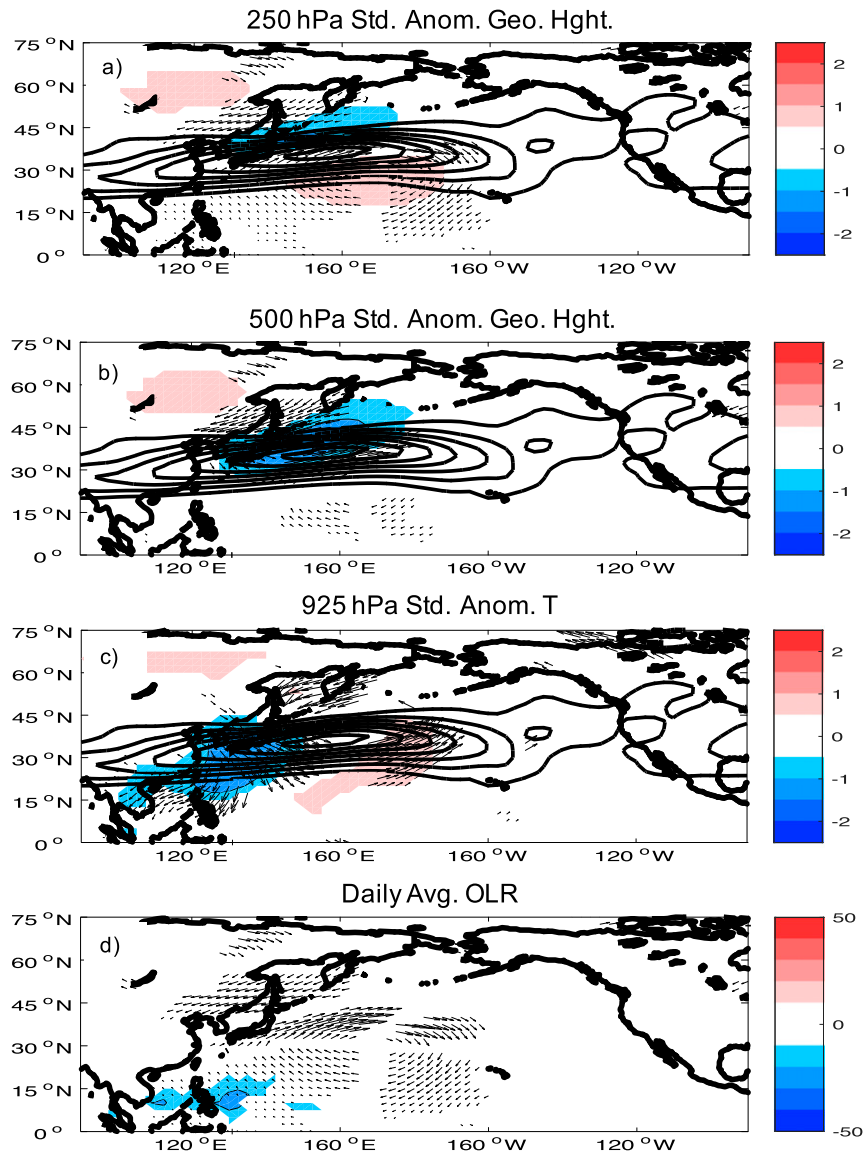


FIG. 2. Adopted from Handlos and Martin (2016). Composite large-scale features at the time of composite west Pacific vertical jet superposition (i.e., time $t = 0$). Shaded regions show positive (negative) standardized anomalous (a) $\phi_{250\text{hPa}}$, (b) $\phi_{500\text{hPa}}$, (c) $T_{925\text{hPa}}$, and (d) daily averaged anomalous (nonstandardized) OLR. Anomalous (nonstandardized) winds are shown as black vectors, with the anomalous winds in (d) being the same as those shown in (a). The black contours represent 250 hPa composite isotachs every 10 m s^{-1} starting at 30 m s^{-1} . Only anomalous values exceeding the 95% confidence limit are plotted.

surge, advects cold air from Siberia southward toward the South China Sea (e.g., Chin 1969; Morrice 1973; Chang et al. 1979; Chang and Lau 1980; Boyle and Chen 1987; Lau and Chang 1987; Zhang et al. 1997; Chan and Li 2004). These cold-air outbreaks, which typically are classified as either “northerly” or “easterly” cold surges (Wu and Chan 1995), play a role in enhancing preexisting convection within the South China Sea region (Johnson and Priegnitz 1981), which can reinforce the west Pacific jet entrance region circulation near Japan; this has also been referred to as the “local Hadley cell circulation”

within this region (e.g., Chang et al. 1979; Chang and Lau 1980). East Asian winter monsoon cold surges are influenced by synoptic-scale events, such as frontal passages (Chang et al. 1983), and have also been shown to be influenced by large-scale teleconnections, such as the Madden–Julian oscillation (e.g., Chang et al. 2005) and El Niño–Southern Oscillation (e.g., Zhang et al. 1997; Wang and Chen 2014).

Specifically, with respect to the effects of the East Asian winter monsoon on the polar–subtropical vertical jet superposition in the west Pacific, the composite superposed jet

structure observed in [Handlos and Martin \(2016\)](#) was shown to be associated with a mid- to upper-tropospheric positive and negative couplet of anomalous geopotential height features straddling the jet core meridionally (Figs. 2a,b). A negative anomaly in geopotential height implies a positive anomalous PV feature (and vice versa); hence these features can be referred to as a PV “couplet.” A northerly cold surge tied to the East Asian winter monsoon moves equatorward prior to jet-superposition occurrence (Fig. 2c), strengthening anomalous convection observed over the South China Sea and the Philippines. Low-PV air associated with the outflow from this convection is advected toward the anticyclonic shear side of the west Pacific jet, enhancing a preexisting positive pressure depth anomaly (equivalently a negative PV anomaly) within the isentropic layer housing the subtropical jet (see Figs. 13–14 of [Handlos and Martin 2016](#)). The pressure depth anomaly is associated with anomalous anticyclonic flow which strengthens the wind speed within the jet core. [Handlos and Martin \(2016\)](#) showed that the juxtaposition of such pressure depth anomalies with geostrophic cold-air advection along the axis of the jet entrance region leads to the development of the vertical PV “wall” characteristic of a vertical jet superposition.

While [Handlos and Martin \(2016\)](#) established a framework for understanding the precursor large-scale environments associated with jet superposition in the west Pacific (including understanding of the relationship between superposition events and the East Asian winter monsoon in this region), the subsequent life cycle of the superpositions and the evolution of their associated large-scale environments *after* superposition have not been investigated. Improving understanding of this post-superposition stage is beneficial for three reasons. First, such investigation will lead to a fuller understanding of the life cycle of robust vertical jet-superposition events. Second, understanding the life cycle will provide insight regarding the influence the large-scale features associated with jet superposition exert on the general circulation of the Northern Hemisphere.

Last, recent research has shown that vertical jet-superposition events have been associated with high-impact weather events. For example, [Christenson and Martin \(2012\)](#) examined the relationship between a west Pacific jet-superposition event and its role in influencing the large-scale upper-tropospheric flow tied to the 25–28 April 2011 southeastern U.S. severe weather outbreak. U.S. tornado outbreaks are shown to be stronger when associated with jet-superposition events versus events where only one of the two jets is involved ([Kelnosky et al. 2018](#)). Anomalous poleward moisture flux from the Gulf of Mexico in response to a jet superposition over the southeastern United States played a key role in the 1 May 2010 Nashville, Tennessee, flood event ([Winters and Martin 2014](#)), while enhanced jet exit region dynamics in response to a developing jet superposition over the same region influenced the development of a significant mid-Atlantic blizzard ([Winters and Martin 2016, 2017](#)).

The above examples demonstrate that improving understanding of vertical jet-superposition development and its relationship to extreme weather in the Northern Hemisphere will enhance understanding of how jet-superposition events

influence weather systems and the large-scale atmospheric circulation relative to the separate polar and subtropical jet streams. For example, [Christenson et al. \(2017\)](#) show that jet superpositions are associated with, on average, wind speeds that are significantly faster than the average wind speeds of both the polar and subtropical jets. This can lead to stronger accelerations associated with jet-superposition jet streaks, which enhance the magnitude of the secondary circulations associated within the jet entrance and exit regions, thus driving stronger synoptic-scaling forcing for the development and maintenance of extratropical cyclones.

Motivated by the three reasons explained above, the goal of this study is to expand upon the analysis of [Handlos and Martin \(2016\)](#) and develop a more complete understanding of the synoptic-scale evolutions tied to west Pacific vertical jet-superposition events throughout their life cycle and the connection of these jet-superposition events to the large-scale atmospheric circulation in the Northern Hemisphere. Investigation of this topic will further enhance the understanding of how these superposition events differ from that of the climatological nonsuperposed west Pacific jet stream. [Section 2](#) describes the methodology used in this study. [Section 3](#) discusses the evolution of the composite jet superposition in the days after initial superposition. This includes discussion of the following: 1) the life cycle of robust west Pacific vertical jet-superposition events, 2) the robustness of the composite evolutions associated with the superposition life cycle, and 3) the structural evolution of the jet. [Section 4](#) explores the evolution of west Pacific jet superpositions in the context of the dominant modes of variability of the west Pacific jet stream. [Section 5](#) concludes the study and suggests foci for future work.

2. Data and methodology

NCEP–NCAR Reanalysis 1 data ([Kalnay et al. 1996](#)) is utilized for all variables and calculations involved in this study. The data have a 2.5° horizontal grid spacing and 6-hourly temporal resolution. Data on both isobaric (unevenly spaced between 100 and 1000 hPa) and isentropic surfaces (interpolated every 5 K and examined in the 315–330 and 340–355 K layers) are used. The 315–330 and 340–355 K layers were computed by averaging all levels between 315–330 and 340–355 K, respectively. Given that this study utilizes the same methodology as that of [Handlos and Martin \(2016\)](#), including the jet-superposition identification scheme (introduced in the next subsection), the NCEP–NCAR Reanalysis 1 dataset is used here to allow for direct comparison and contrast of results with the 2016 study.

a. Identification of robust west Pacific jet-superposition events

[Table 1](#) shows the 44 robust west Pacific jet-superposition cases identified in [Handlos and Martin \(2016\)](#) during the 31-winter period 1979/80–2009/10 (where boreal winter is defined as the months of December, January, and February with leap days excluded). These superposition events were identified using a jet-superposition identification scheme that evaluates

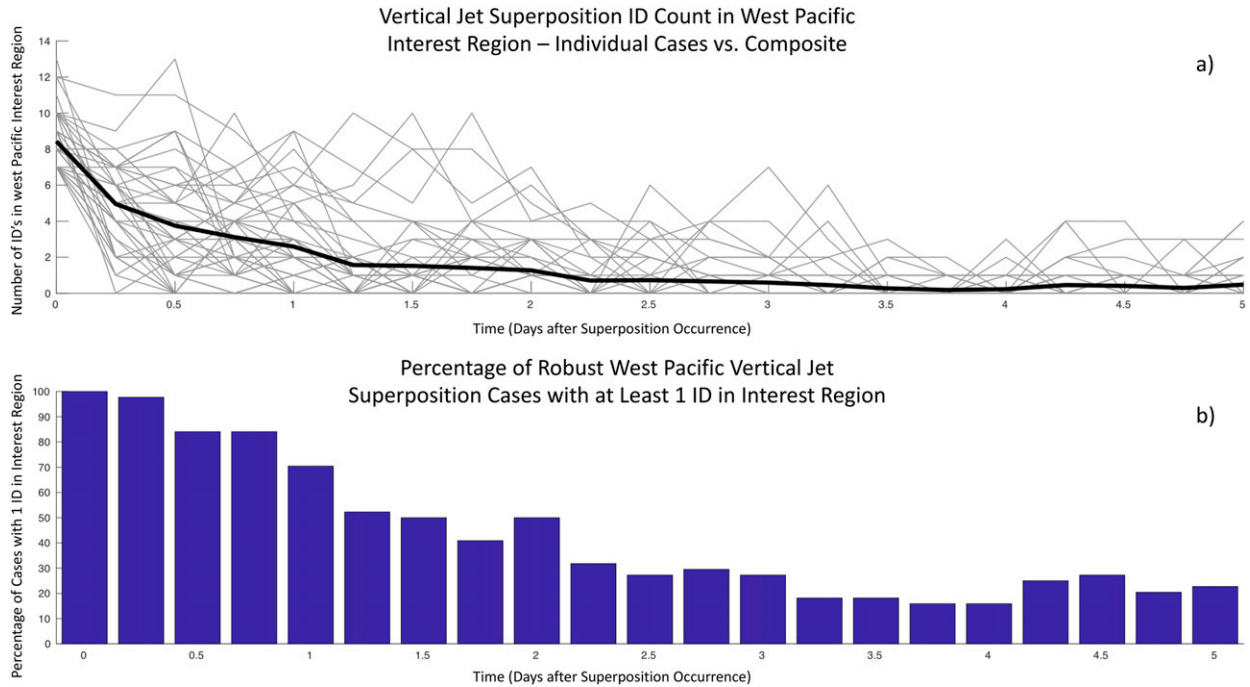


FIG. 3. (a) Number of vertical jet-superposition IDs within the west Pacific interest region at time $t + X$ (where X = days after superposition occurrence) for each of the 44 cases listed in Table 1 (thin gray lines) and the composite superposed jet (thick black line). (b) Percentage of the 44 cases with at least 1 ID within the west Pacific interest region over the same time frame.

characteristics of the PV and wind speed distributions within each grid column over the Northern Hemisphere. Within the 315–330 K (340–355 K) layer, where the polar jet (subtropical jet) has been shown to reside during boreal winter (Christenson et al. 2017), whenever $|\nabla PV|$ within the 1–3 PVU ($1 \text{ PVU} = 10^{-6} \text{ K kg}^{-1} \text{ m}^2 \text{ s}^{-1}$) channel exceeds or is equal to a threshold value (e.g., the threshold value is $0.64 \times 10^{-5} \text{ PVU m}^{-1}$ for both layers) and the integral average wind speed in the 400–100 hPa layer exceeds 30 m s^{-1} , a polar (subtropical) jet is identified in that grid column. A vertical jet-superposition event (JSID) is identified if both the polar and subtropical jet criteria are met within the same grid column.

For a date/time to be considered a “robust” event, seven or more JSIDs are required to occur within a limited region of the west Pacific (defined as $30^\circ\text{--}40^\circ\text{N}$, $135^\circ\text{--}175^\circ\text{E}$) at a 6-hourly analysis time (boxed region in Fig. 1f). We define the time of jet-superposition occurrence, $t = 0$, as the time at which the above criterion is met subject to the following additional conditions: 1) that the total number of JSIDs occurring 6 h before the identified 6-hourly time is less than the number of JSIDs observed at the time of superposition, and 2) that the total number of JSIDs occurring 6 h after the identified 6-hourly time is less than or equal to the number of JSIDs observed at the time of superposition. This is the same criteria that were used in Handlos and Martin (2016) for identifying jet-superposition events of interest in this region. While one critique to this methodology is that 13 of the 44 cases within the composite analysis are within 12 h of each other, removal of such potential “overlapping” events does not significantly change the results discussed later in this study (not shown).

Furthermore, the authors wish to maintain consistency between the results of this study and Handlos and Martin (2016) to allow for direct comparison and contrast.

b. Composite analysis

We utilize the composite analysis method of Handlos and Martin (2016) to investigate the temporal evolution of west Pacific jet-superposition events and their associated large-scale features after $t = 0$. We construct composite maps containing either anomalies or standardized anomalies as follows:

$$X_{\text{std.anom.}} = \frac{X_{\text{supj}} - X_{\text{climo}}}{X_{\text{stdclimo}}}, \tag{1}$$

where $X_{\text{std.anom.}}$ is the standardized anomaly of a variable for a jet-superposition event, X_{supj} is the variable measured at the point of interest at the 6-h time of interest for a jet-superposition event, X_{climo} is the 31-winter mean of the variable at the 6-h time, and X_{stdclimo} is the climatological standard deviation of the 31-winter climatology of variable X at that 6-h time.

3. West Pacific jet-superposition events after time of superposition

a. Lifetime of west Pacific jet-superposition events

Figure 3a shows a time series of the number of JSIDs within the west Pacific interest region in the 5 days after $t = 0$ for all 44 cases identified as well as for the composite superposed jet. Given the constraints applied in identifying robust west Pacific

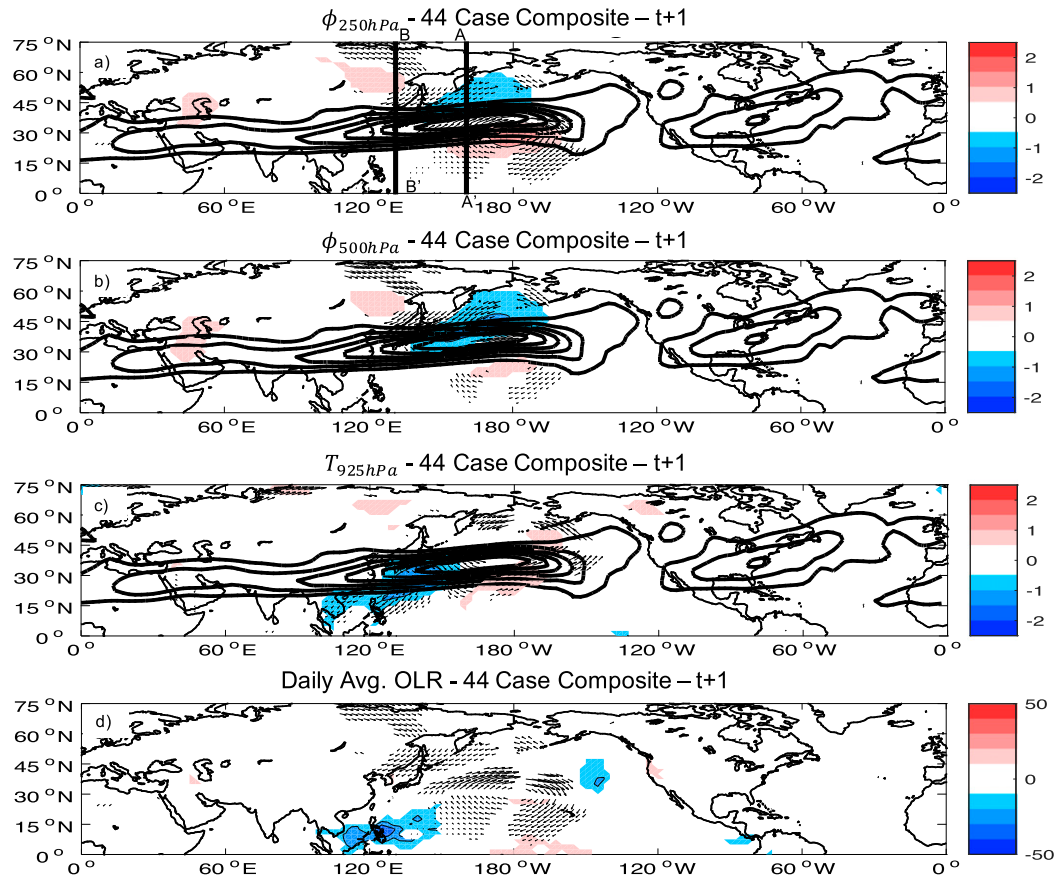


FIG. 4. As in Fig. 2, but 1 day after composite west Pacific jet superposition (i.e., time $t + 1$ day). Note that the domain has been expanded to show all longitudes within the Northern Hemisphere. Line A–A' represents the cross-sectional slice shown in Fig. 12a, and line B–B' represents the cross-sectional slices shown in Figs. 14 and 15.

vertical jet-superposition events, the number of JSIDs that occur in the west Pacific interest region on average (8.4 JSIDs) decreases significantly 6 h after superposition occurrence (i.e., 5.0 JSIDs). At 1 day after superposition, the average number of identifications decreases to 2.6 JSIDs, decreasing further to 1.3 JSIDs and 0.6 JSID 2 and 3 days after jet-superposition occurrence, respectively.

Figure 3b shows the percentage of jet-superposition events that have at least 1 JSID within the west Pacific interest region from time $t = 0$ to $t + 5$ days. At time $t + 1$ day, the percentage of 44 robust superposition cases with 1 ID decreases to 70.5% (31 JSIDs), 50.0% (22 JSIDs) by time $t + 2$ days and 27.3% (12 JSIDs) by time $t + 3$ days. Defining the “end” of a jet-superposition event as the time after robust jet-superposition occurrence in which 0 IDs occur within the west Pacific interest region (not shown), we find that 61.4% of cases (i.e., 27 cases) last at least 1 day, 25.0% (i.e., 11 cases) last at least 2 days and 9.09% (i.e., 4 cases) last at least 3 days, with the average length of a robust west Pacific jet-superposition event being 1.26 days.

In summary, Fig. 3 shows that west Pacific vertical jet-superposition events are shorter in duration than the typical 5–7 day time scale of the life cycles of synoptic-scale weather systems (e.g., see p. 113 of Martin 2012). This fact emphasizes

how dependent jet-superposition events are on the synergistic nature of the physical processes that characterize an environment favorable for jet-superposition development. In other words, jet-superposition events are most likely to occur when the key synoptic-scale evolutions that induce and maintain jet-superpositions in the west Pacific occur together within this narrow 1–2 day time frame.

b. Composite environments associated with west Pacific jet-superposition events post-superposition

Figures 4–7 depict standardized anomalous quantities of interest with respect to composite robust west Pacific vertical jet-superposition events 1–4 days after composite jet-superposition occurrence, respectively. In these figures, only statistically significant values at the 95% confidence level based on a two-tailed Student's t test are plotted. With respect to anomalous wind, only vectors where both the zonal and meridional wind components exceed the 95% limit are shown. At time $t + 1$ day (Fig. 4), the composite superposed jet has extended eastward and weakened to a maximum wind speed between 80 and 90 m s^{-1} . Figure 4a shows a strengthening of the positive $\phi_{250\text{hPa, std. anom.}}$ anomaly relative to the previous composite day (i.e., Fig. 2a), and this feature remains associated

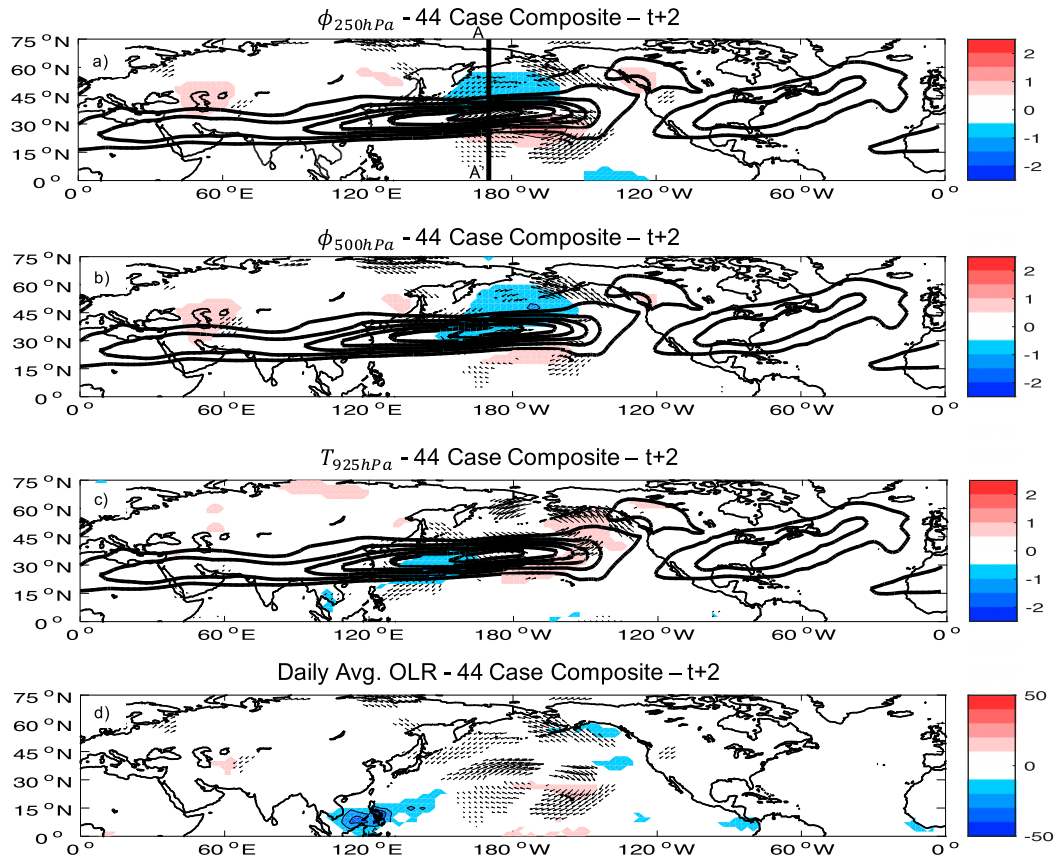


FIG. 5. As in Fig. 4, but 2 days after composite west Pacific jet superposition (i.e., time $t + 2$ days). Line A–A' represents the cross-sectional slice shown in Fig. 12b.

with strong anomalous anticyclonic flow. The anomalous negative ϕ on the cyclonic shear side of the composite jet remains about the same magnitude (i.e., around -0.5σ) at 250 and 500 hPa (Figs. 4a,b). Figure 4c shows that the anomalous cold air associated with anomalous northerly winds over the East and South China Seas still persists, though by this time the feature has started to shift eastward as the jet extends eastward. Anomalous negative OLR¹ values (a proxy for enhanced convective activity) remain anchored near the Philippines (Fig. 4d). However, with the eastward movement of the positive $\phi_{250\text{hPa, std. anom.}}$ feature equatorward of the jet, the anomalous southwesterlies in the upper troposphere that were in a position to advect the low-PV air of the convective outflow away from the Maritime Continent region at time $t = 0$ are now shifting away from the anomalous convection.

Throughout the rest of the Northern Hemisphere, there are very few locations where any of the variables plotted exceed $\pm 0.5\sigma$ (or $\pm 10 \text{ W m}^{-2}$ for anomalous OLR) and are statistically significant. A composite jet with wind speed maximum around 50 m s^{-1} resides over the East Coast of the United States, though the wind anomalies associated with this jet do not exceed 0.5σ (not shown). Thus, at time $t + 1$ day, the

majority of standardized anomalous large-scale elements exceeding the 0.5σ threshold are located near the west Pacific superposed jet.

At time $t + 2$ days (Fig. 5), the composite jet continues to extend eastward, maintaining about the same magnitude within its core. The jet over the western Atlantic has remained relatively stationary, weakening slightly. While the positive and negative $\phi_{250\text{hPa, std. anom.}}$ and $\phi_{500\text{hPa, std. anom.}}$ features remain relatively unchanged at this time (with a slight weakening of the negative ϕ anomaly at 500 hPa), these features reside within the right and left jet exit regions as the jet extends (Figs. 5a,b). The composite cold-surge feature has now weakened substantially, with remnant anomalous northerly winds and cold air present northeast of Indonesia (Fig. 5c). Anomalous warm air associated with anomalous southerly winds south and east of the center of the upper-tropospheric anomalous cyclonic circulation within the left jet exit region is observed south of Alaska. Centered along coastal British Columbia, anomalous positive ϕ in the mid- to upper troposphere indicates the presence of a composite anomalous ridge, though the flow itself near this anomaly does not exhibit statistical significance. Finally, both the areal extent and magnitude of anomalous convection in the Maritime Continent region, is largely unchanged (Fig. 5d). With the anomalous convection and its outflow dissociated from the

¹ OLR data are anomalies from the NCEP–NCAR Reanalysis 1 data.

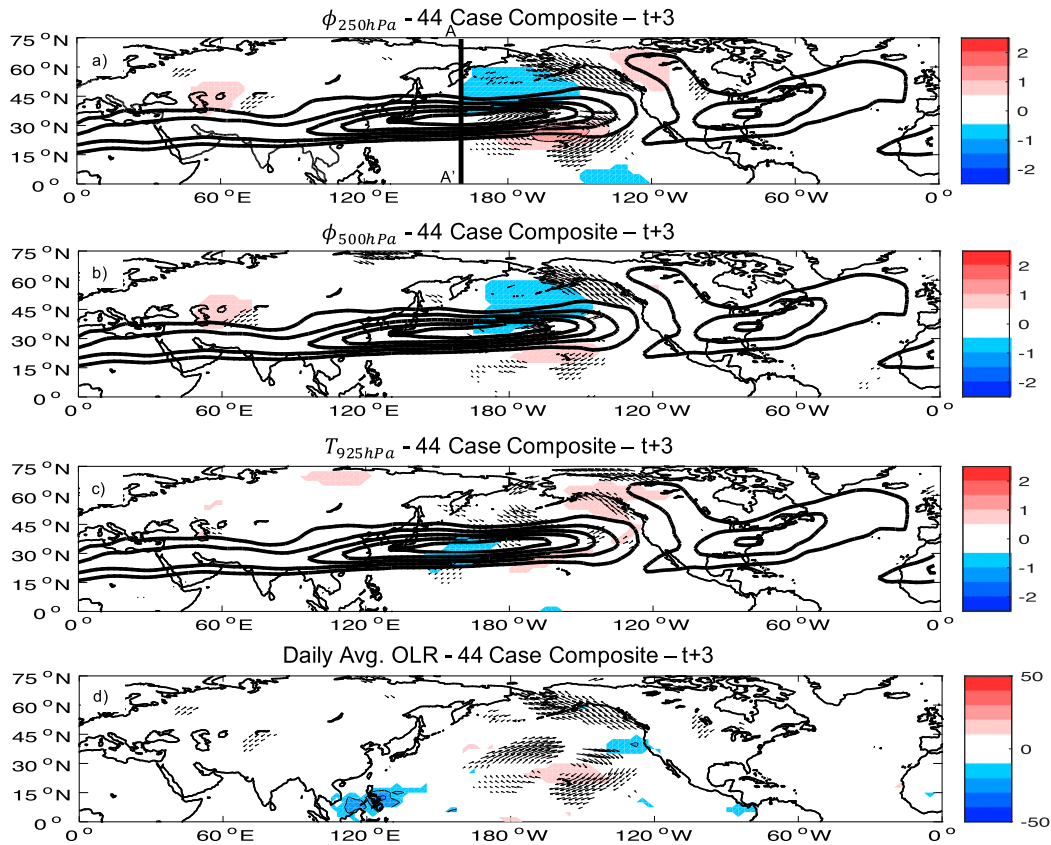


FIG. 6. As in Fig. 4, but 3 days after composite west Pacific jet superposition (i.e., time $t + 3$ days). Line A–A' represents the cross-sectional slice shown in Fig. 13a.

upper-tropospheric anomalous anticyclonic flow on the anticyclonic shear side of the jet, the advection of low-PV air from the region of convection is no longer a primary forcing supporting composite west Pacific jet superposition.

At time $t + 3$ days (Fig. 6), the core of the composite jet continues to extend eastward. The anomalous ϕ features within the jet exit regions are still present in the 250 and 500 hPa composites and remain within the jet exit regions throughout the jet extension (Figs. 6a,b). Figure 6c shows the remnants of the anomalous cold surge propagating eastward, with the region of cold air $\leq -0.5\sigma$ decreasing in area. A warm-air anomaly associated with the ridge over Alaska still persists, while the warm-air anomaly region southeast of the west Pacific jet core shrinks in size. The region of negative OLR values near Indonesia continues to shrink as well (Fig. 6d).

Finally, at time $t + 4$ days (Fig. 7), the majority of the large-scale elements referenced earlier have weakened. For example, the maximum wind speed associated with the composite jet decreases, though the jet does continue to extend farther eastward. The ϕ anomalies at 250 and 500 hPa remain comparably vigorous while shifting slightly eastward with the extension of the jet (Figs. 7a,b). The composite standardized anomalous temperature $< 0.5\sigma$ has nearly disappeared (Fig. 7c) as has the warm-air feature in the jet exit region. The lower-tropospheric warm-air anomaly first noted at time

$t + 2$ days over eastern Alaska is still present over eastern Alaska and northwestern Canada at this time. Along with the dissipation of the cold- and warm-air anomalies observed in the jet exit region, both the areal extent and magnitude of negative OLR near Indonesia continue to decrease (Fig. 7d).

In summary, Figs. 4–7 illustrate that the following elements characterize the large-scale environment throughout this 4-day period: 1) an eastward extension of the west Pacific jet, 2) the continued presence of the mid- to upper-tropospheric positive and negative ϕ anomalies, particularly within the right and left jet exit regions, respectively, 3) the dissipation of the anomalous cold-surge event as it propagates eastward across the Pacific Ocean and 4) a progressive disconnect between the anomalous convection and the west Pacific jet. The next subsection quantifies the fraction of individual cases within the composite that exhibit these key features.

c. Frequency of occurrence of key large-scale environmental features and their coherence post-jet superposition

To determine whether the observed standardized anomalous features in the 44-case composite occurred within the majority of cases examined, Handlos and Martin (2016) considered the percent occurrence of cases for each grid point in which the $\pm 0.5\sigma$ threshold was exceeded for several standardized anomalous variables of interest. This same analysis is

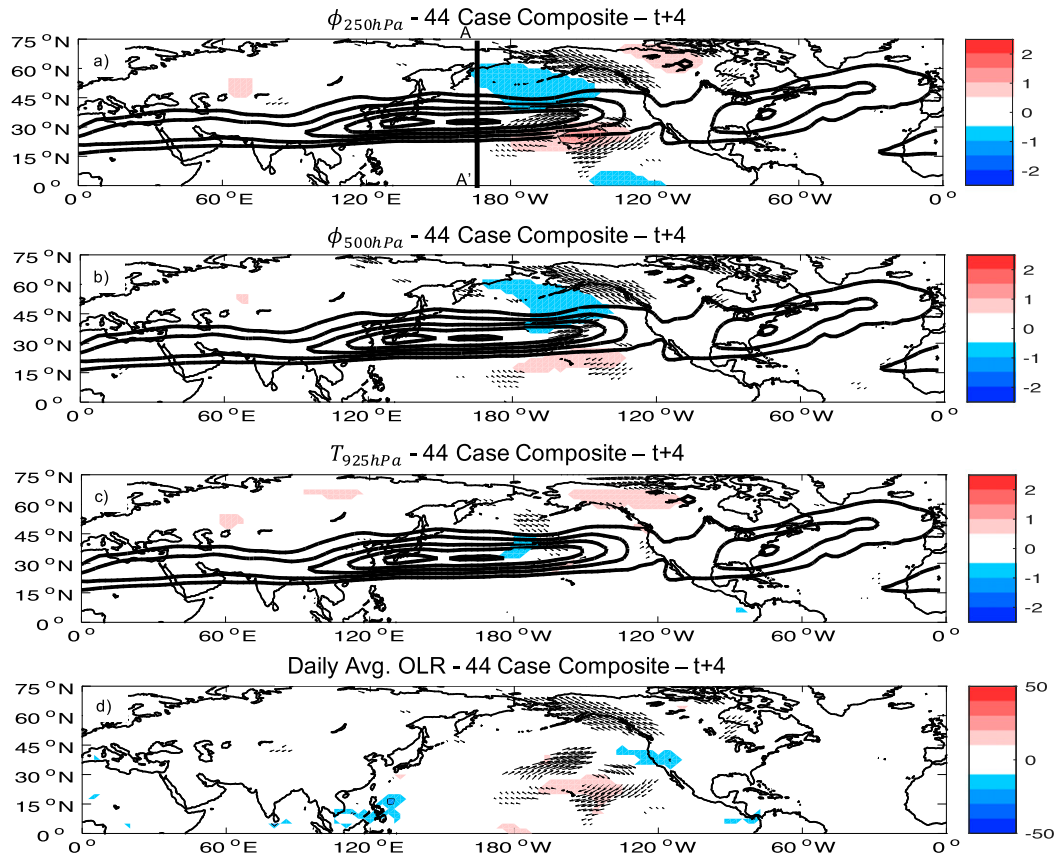


FIG. 7. As in Fig. 4, but 4 days after composite west Pacific jet superposition (i.e., time $t + 4$ days). Line A–A' represents the cross-sectional slice shown in Fig. 13b.

repeated for times $t + 1$ day through $t + 4$ days to determine if the large-scale environments that characterize the composite evolution post-superposition occur within the majority of the 44 cases.

Figures 8–11 show plots of the frequency of occurrence of grid points $\geq \pm 0.5\sigma$ out of the 44 total vertical jet-superposition events used in our composite analysis at the times shown in Figs. 4–7. With respect to positive standardized anomalous $|\mathbf{u}|_{250\text{hPa, std. anom.}}$, 42 of 44 (i.e., 95.5% of) cases fulfill this requirement within the west Pacific jet core at time $t + 1$ day (Fig. 8a). A similarly large fraction ($\geq 70\%$ – 80%) of cases exhibit grid points $\leq -0.5\sigma$ in regions flanking the jet core meridionally. Throughout the evolution of the extension of the composite jet (Figs. 8b–d), the frequency of occurrence for all wind anomalies associated with the extended, narrow jet remains $\geq 60\%$ – 80% . Within the western portion of the jet, the percent occurrence decreases throughout the extension. Thus, while the eastward extension of the jet occurs within the majority of cases included in the composite, significant jet variability exists upstream.

Figure 9 shows that the $\phi_{250\text{std. anom.}}$ feature on the anticyclonic shear side of the composite jet occurs in 41 of 44 (i.e., 93.2% of) cases or more in some grid points as this anomaly moves eastward over time. Interestingly, the number of events where the negative standardized anomalous threshold is met at

250 hPa in the composite left jet exit region increases between $t + 1$ day and $t + 2$ days (Figs. 9a,b), remaining relatively constant even up to time $t + 4$ days (Figs. 9c,d). Thus, the persistence of the anomalous ϕ features within the jet exit region characterizes the majority of cases comprising the composite.

The findings above are also observed at 500 hPa (Fig. 10). The number of cases where $\phi_{500\text{hPa, std. anom.}} \leq -0.5\sigma$ on the cyclonic shear side of the jet (associated with the anomalous trough-like feature) is as high as 41 of 44 (i.e., 93.2% of) cases at time $t + 1$ day (Fig. 10a), with the maximum percent of cases in the core of this anomaly remaining somewhere between $\geq 70\%$ – 80% through time $t + 4$ days. The anomalous positive ϕ feature equatorward of the jet at 500 hPa exceeds the 0.5σ threshold in more cases at time $t + 4$ days than time $t + 1$ day (Figs. 10a versus 10d).

Finally, with respect to the eastward propagation and dissipation of the anomalous cold-surge feature, the number of cases exhibiting anomalous cold air exceeding the 0.5σ threshold decreases consistently over the 4 days (Fig. 11). On the other hand, over 50%–70% of cases are associated with the development of the warm-air anomaly near Alaska throughout the 4-day period. This coincides with a weak signature (based on this metric) of consistent anomalous positive ϕ in the mid- to upper troposphere, where the highest percentage occurrence

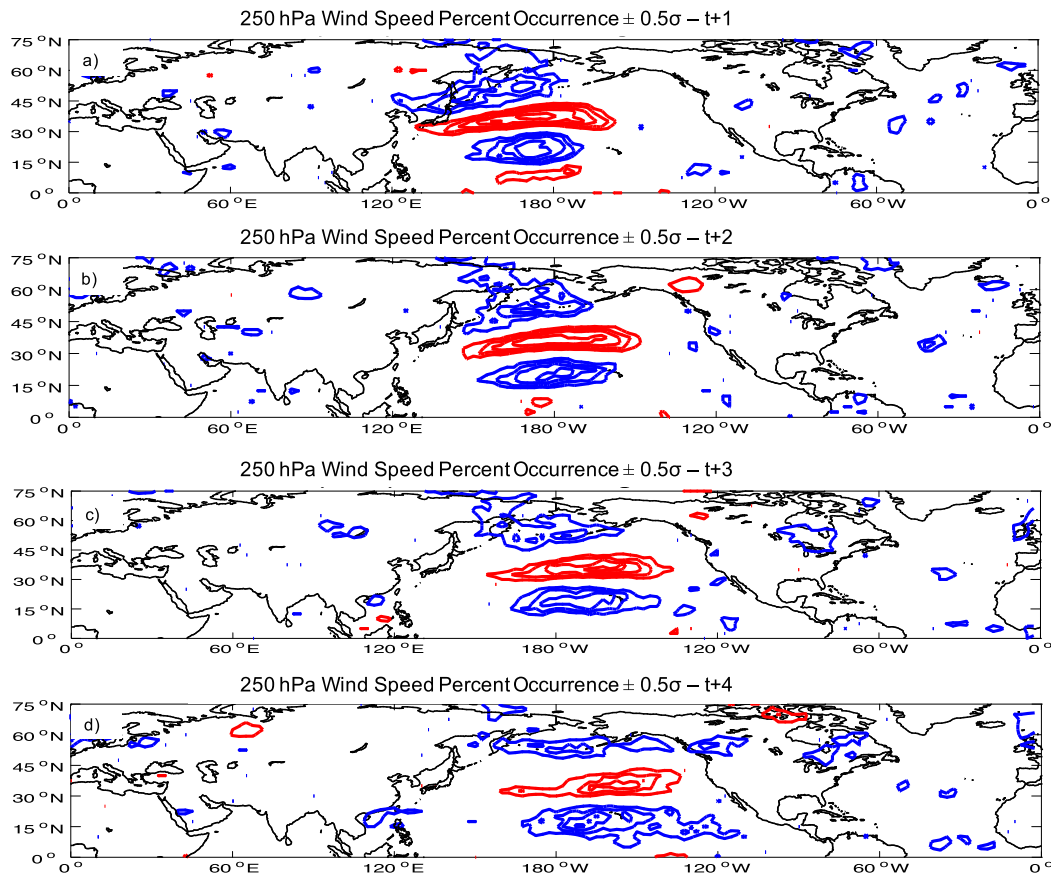


FIG. 8. Percent occurrence of standardized anomalous 250 hPa wind speed for all 44 cases used in the composite at times (a) $t + 1$, (b) $t + 2$, (c) $t + 3$, and (d) $t + 4$ days. Red (blue) contours indicate regions where 250 hPa wind speed with standardized value $\geq 0.5\sigma$ ($\leq -0.5\sigma$) occurs in at least 50% of cases, contoured every 10%.

over the Northwest Territories exceeds 60% of cases at times $t + 2$ and $t + 3$ days (Figs. 9b,c and 10b,c). Therefore, many of the robust superposition cases exhibit anomalous ridging and warming in this region within a few days after superposition.

To summarize, Figs. 8–11 show that the occurrence of an extended jet, anomalous ϕ maximum and minimum features within the composite jet exit regions at 250 and 500 hPa, dissipation of the northerly cold-surge anomaly and anomalous warm air and ridging in Alaska at 925 hPa occur within the majority of the cases included in the composite. The evolution of these features is consistent up to 4 days after superposition occurrence. Thus, results suggest that these features are associated with the evolution of the west Pacific jet post-superposition within the majority of cases considered within the composite analysis.

d. Post-superposition evolution—composite cross-section perspective

Handlos and Martin (2016) showed that the vertical structure of the composite west Pacific jet, when superposed, exhibited the characteristic two-step tropopause structure with a deep, vertical PV wall within the jet core. This PV wall arises from the juxtaposition of 1) low-PV air in the subtropical jet

isentropic layer exhausted from convection equatorward of the jet core, and 2) high-PV air associated with subsidence forced by geostrophic cold-air advection in cyclonic shear within the jet entrance region (see Handlos and Martin 2016, Fig. 17). Coincidentally, the authors observed an anomalously strong jet entrance region circulation at the time of jet-superposition occurrence. In this section, composite cross sections through the jet core and jet entrance regions are again considered but in the context of the post-superposition evolution of the vertical structure of the composite jet.

Figures 12 and 13 show cross sections taken through the west Pacific jet core at times $t + 1$ day through $t + 4$ days (see Figs. 4a–7a for cross-sectional slices A–A', which change longitude slightly in order to capture the core of the composite superposed jet). At times $t + 1$ day and $t + 2$ days, the characteristic vertical PV “wall” associated with a positive and negative anomalous PV couplet flanking the jet core, as observed at $t = 0$ in Handlos and Martin (2016), is still present (Figs. 12a,b). This is because the western edges of the positive and negative geopotential height anomalies flanking the jet core are still present within the cross-section region. However, at times $t + 3$ and $t + 4$ days, the magnitude of the positive and negative Ertel PV anomalies on the poleward and equatorward

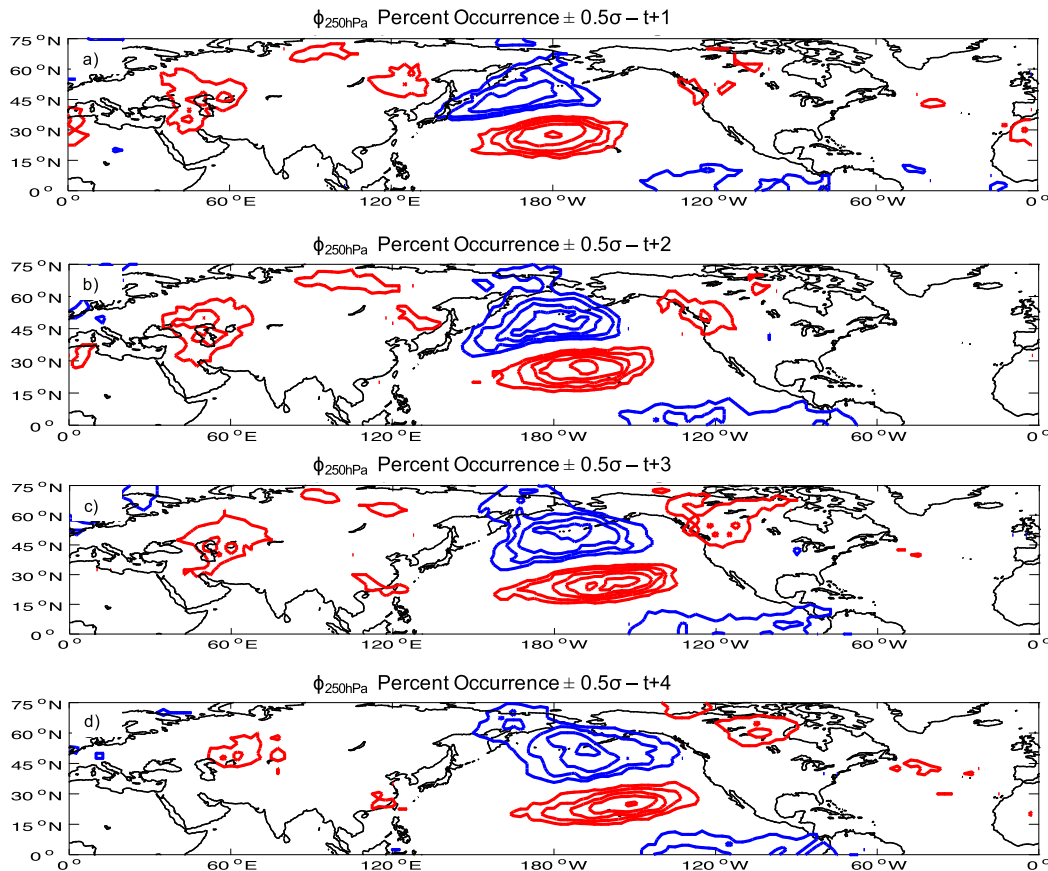


FIG. 9. As in Fig. 8, but for standardized anomalous $\phi_{250\text{hPa}}$.

sides of the jet core weaken and retreat to higher elevations (Figs. 13a,b). This is associated with the eastward propagation of the positive and negative upper-tropospheric geopotential height anomalies away from the core of the composite superposed jet into the composite jet exit regions. Furthermore, with the weakening of the anomalous negative OLR feature over the Maritime Continent region, low-PV air is no longer being advected into this layer post-superposition (as discussed earlier with respect to Fig. 5). As a result of the above, geopotential heights increase (decrease) on the cyclonic (anticyclonic) shear side of the composite jet such that the tropopause height structure regresses back toward climatology, exhibiting a less steep vertical tropopause wall (Fig. 7a in Handlos and Martin 2016). Also, with a weaker gradient in tropopause height, the maximum wind speed within the composite jet core weakens from > 90 to $< 80 \text{ m s}^{-1}$, thus also approaching climatological values within this region.

Figures 14 and 15 show cross sections taken through the west Pacific jet entrance region at times $t + 1$ day through $t + 4$ days (see Fig. 4a for cross-sectional slice B–B'), highlighting anomalous vertical motion. At time $t + 1$ day (Fig. 14a), anomalous upward vertical motion is exhibited south of the composite jet entrance region, while anomalous downward vertical motion is exhibited beneath the composite jet entrance region. This demonstrates that the equatorward shifted anomalous thermally

direct circulation characteristic of the composite vertically superposed jet is still present. At time $t + 2$ days (Fig. 14b), the magnitude of downward vertical motion weakens and is shifted farther equatorward. This weakening is associated with the weakening in magnitude of geostrophic cold-air advection along the axis of the jet entrance region over this 48-h time period (Figs. 16a,b). Weaker geostrophic cold-air advection post-superposition implies less subsidence and less lowering of the tropopause height north of the jet, aiding in the regression of the vertical jet structure back to its climatological state.

At times $t + 3$ and $t + 4$ days (Figs. 15a,b), the anomalous equatorward-shifted thermally direct circulation associated with the jet entrance region continues to weaken in magnitude. Similar to time $t + 2$ days, at times $t + 3$ and $t + 4$ days, the magnitude of geostrophic cold-air advection within the jet entrance region weakens within the vicinity of the cross section (Figs. 16c,d). As a result of the weakening of this circulation, the subsidence that was present beneath of the jet core, along with the upward vertical motion that was observed south of the jet core, at the time of composite vertical jet superposition are less influential in decreasing the tropopause height poleward and increasing the tropopause height equatorward of the core of the jet entrance region, respectively. Thus, the jet structure at the end of the 96-h sequence continues to regress toward its mean state.

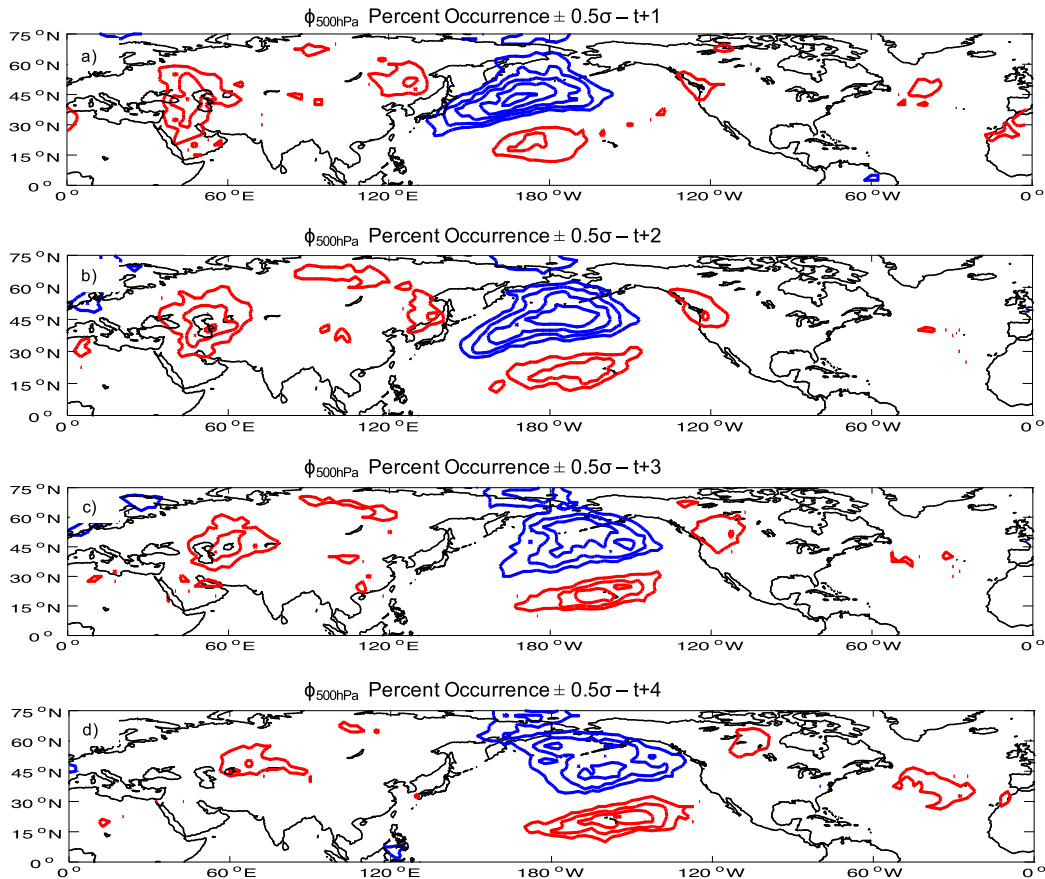


FIG. 10. As in Fig. 8, but for standardized anomalous $\phi_{500\text{hPa}}$.

In summary, the cross sections through the 44-case composite west Pacific jet core and entrance regions post-superposition reveal the following: (i) A less vertically oriented PV wall associated with a weakening of both positive and negative geopotential height anomalies flanking the jet core and (ii) a weakening of the anomalous thermally direct circulation associated with the composite jet entrance region. The weakening of the composite vertical jet-superposition structure is tied to: (i) the eastward propagation of both negative and positive geopotential height anomaly features as the jet extends eastward, (ii) the lack of anomalous anticyclonic flow equatorward of the jet to advect low-PV air toward the jet core and (iii) the weakening of geostrophic cold-air advection along of the jet entrance region axis. These findings show the importance of the flanking geopotential height anomalies, advection of low-PV air into the subtropical jet isentropic layer and geostrophic cold-air advection along the composite jet entrance region axis with respect to *both* the development and maintenance of a jet-superposition event.

4. Jet-superposition extension and poleward extent and relationship to the large-scale circulation

The extension (or retraction) of the west Pacific jet has been shown to be associated with several teleconnection phenomena.

This includes (but is not limited to) the Pacific–North American (PNA) pattern, extreme precipitation events in the Pacific including the western United States, kona low events near Hawaii, and significant ridge-building events near Alaska (e.g., Chu et al. 1993; Kodama and Barnes 1997; Otkin and Martin 2004; Jaffe et al. 2011; Griffin and Martin 2017). Research has also demonstrated a connection between Madden–Julian oscillation tropical convection with extratropical circulation anomalies that affect the position and strength of the west Pacific jet (e.g., Liebmann and Hartmann 1984; Lau and Phillips 1986; Livezey and Mo 1987; Sardeshmukh and Hoskins 1988; Kushnir and Wallace 1989; Schubert and Park 1991; Mo and Kousky 1993; Anderson and Rosen 1983; Weickmann et al. 1985; Knutson and Weickmann 1987; Matthews and Kiladis 1999; Moore et al. 2010) as well as the effects of tropical cyclones (Archambault et al. 2013). Given that the composite results reveal that robust west Pacific vertical jet-superposition events characteristically lead to an extension of the west Pacific jet stream, and given the influence that the west Pacific jet has on Northern Hemisphere atmospheric circulation, it is of interest to determine if any relationship exists between metrics used to determine the evolution of the west Pacific jet with that of the results from the composite analysis. Specifically, the evolution of west Pacific jet extension/retraction and meridional shift are explored, as investigating

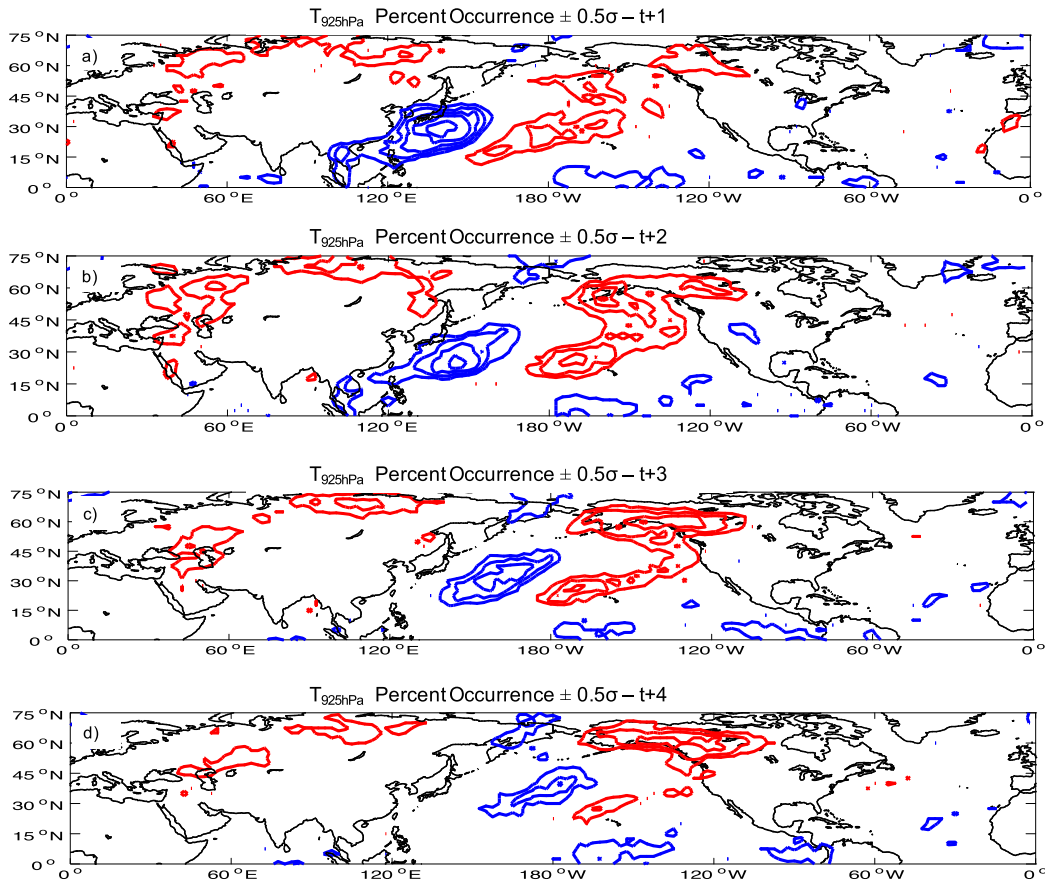


FIG. 11. As in Fig. 8, but for standardized anomalous $T_{925\text{hPa}}$.

this could prove beneficial in tracking the evolution of west Pacific jet-superposition events and associated changes to the large-scale Northern Hemisphere circulation.

To quantify jet extension (or retraction) with respect to west Pacific vertical jet-superposition events, we adapt the methodology of Jaffe et al. (2011) and Delcambre et al. (2013) and extract the two leading modes of Pacific jet variability by performing a principal component analysis (PCA) on 300 hPa zonal wind over the basin (i.e., 20°–80°N, 100°E–60°W). This analysis employs daily average data, includes the months of November and March, and applies a 5 day running mean to filter out high-frequency variability. The two most dominant modes of jet variability are the following: 1) The zonal extension or retraction of the exit region of the west Pacific jet and 2) the poleward or equatorward shift of the jet over the west and central Pacific (not shown). These modes are consistent with prior studies that utilize PCA to explore west Pacific jet variability (e.g., Athanasiadis et al. 2010; Griffin and Martin 2017; Winters et al. 2019b). The principal components (PCs) of each mode are used to investigate their evolution with time.

A notable observation from this analysis is that significant variability exists among the 44 individual cases with respect to the evolution of the PCA modes. This is demonstrated by the variability in the location of PC1/PC2 values for each west Pacific vertical jet-superposition event at times $t - 5$, $t = 0$, and

$t + 5$ days (Figs. 17a–c). For example, at $t - 5$ days (Fig. 17a), the number of superposition cases that fall within the “retracted–poleward shifted” (top-left; PC1 < 0 and PC2 > 0), “extended–poleward shifted” (top-right; PC1 > 0 and PC2 > 0) and “extended–equatorward shifted” (bottom-right; PC1 > 0 and PC2 < 0) quadrants are similar; only 5 cases fall within the “retracted/equatorward shifted” (bottom-left; PC1 < 0 and PC2 < 0) quadrant at this time. At $t = 0$ (Fig. 17b), although variability in PC1/PC2 value is still evident, the cases suggest convergence toward the “jet extension–poleward shift” (i.e., upper-right) quadrant. By $t + 5$ days (Fig. 17c), the majority of cases reside within the “extended/poleward shifted” quadrant (i.e., 26 of 44 cases). At this time, 34 of 44 cases exhibit PC1 > 0, indicating an extended jet, and 34 of 44 cases exhibit PC2 > 0. Figure 17 overall shows that, while significant variability exists between the 44 cases with respect to their extension or retraction and poleward or equatorward shift, overall, the large-scale environments that produce robust west Pacific jet superposition tend to modify the jet into an extended and slightly poleward deflected state to some extent. However, while the two most dominant modes of variability have been shown to perform well at tracking the evolution of the west Pacific jet in other circumstances, with respect to jet-superposition events, variability with respect to jet-superposition evolution may be too

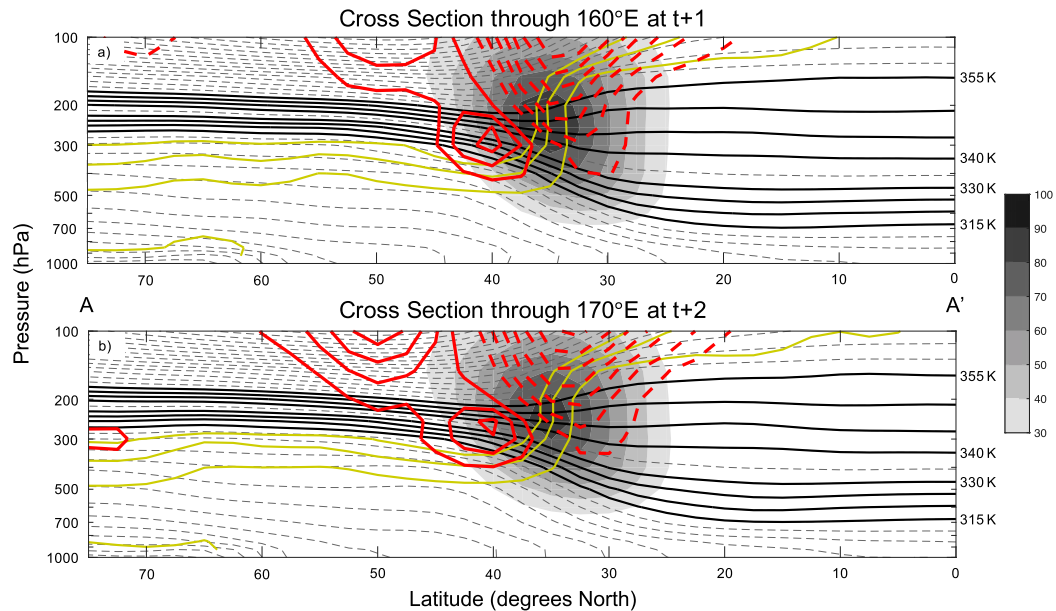


FIG. 12. Composite cross sections through the core of the composite vertically superposed jet in the west Pacific. Each cross section shows wind speed (gray fill; 10 m s^{-1} intervals starting at 30 m s^{-1}), isentropic surfaces (dashed gray contours every 5 K starting at 280 K, with levels within 315–330 and 340–355 K layers in solid black contours), the 1–3 PVU channel in the upper troposphere (solid yellow contours; PVU), and anomalous Ertel PV [solid (dashed) red contours every 0.5 PVU starting at +0.5 (–0.5) PVU]. The cross-sectional locations and times are as follows: (a) along 160°E at time $t + 1$ day and (b) along 170°E at time $t + 2$ days. Each cross section is marked in (a) of Figs. 4 and 5 (A–A' lines).

large for this metric to exhibit any consistent jet-superposition evolution during the jet-superposition life cycle.

Jaffe et al. (2011) (e.g., their Fig. 9b) and Griffin and Martin (2017) (e.g., their Fig. 4c), investigating west Pacific jet PC

modes 1 and 2 via EOF and time-extended EOF analysis, respectively, showed that anomalous cyclonic and anticyclonic flow resides within the left and right exit regions of the jet during west Pacific jet extension. Both studies also

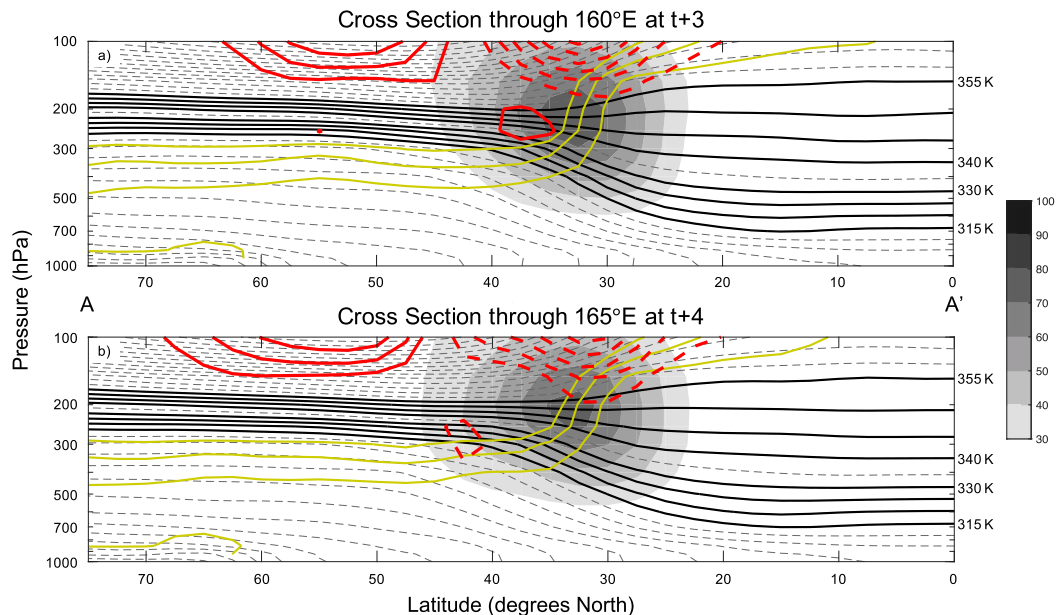


FIG. 13. As in Fig. 12, but for cross sections (a) along 160°E at time $t + 3$ days and (b) along 165°E at time $t + 4$ days. Each cross section is marked in (a) of Figs. 6 and 7 (A–A' lines).

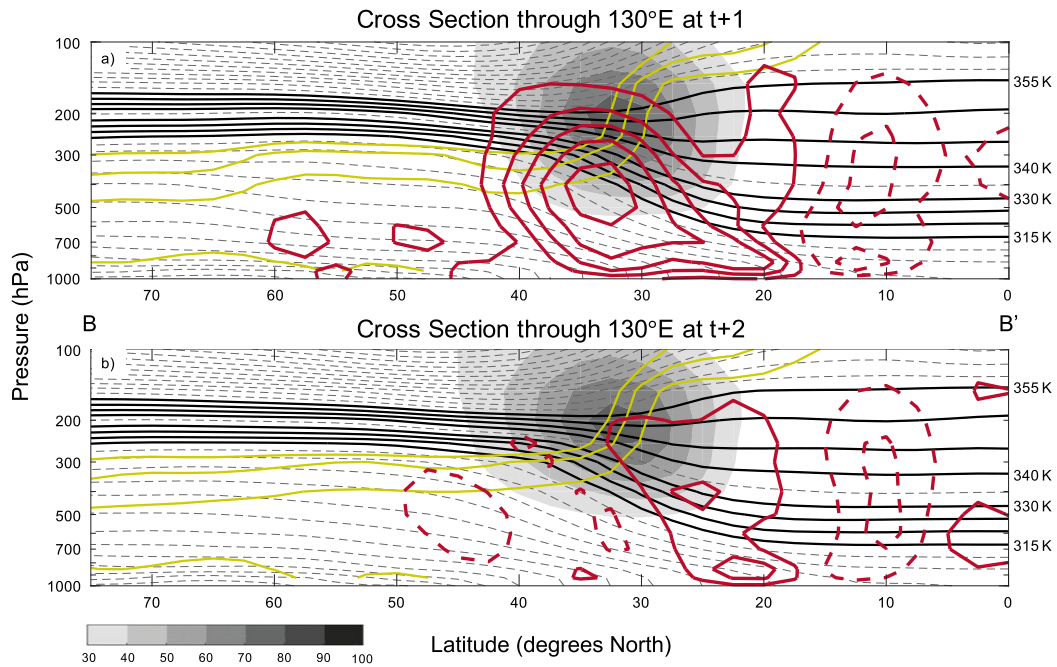


FIG. 14. Composite cross sections taken along 130°E longitude (B–B' line in Fig. 4a) at time (a) $t + 1$ day and (b) $t + 2$ days. All conventions are as in Figs. 12 and 13, but the maroon solid (dashed) contours represent anomalous downward (upward) vertical motion every 0.025 Pa s^{-1} starting at $+0.01$ (-0.01) Pa s^{-1} .

demonstrate ridge building near Alaska during west Pacific jet extension. These findings are consistent with our post-superposition composite results despite the significant variability exhibited between individual cases.

Furthermore, Griffin and Martin (2017) show that anomalous cold air is present 5 days prior to maximum jet extension occurrence, and anomalous convection is present within the Maritime Continent at times $t - 5$, $t = 0$, and $t + 5$ days relative

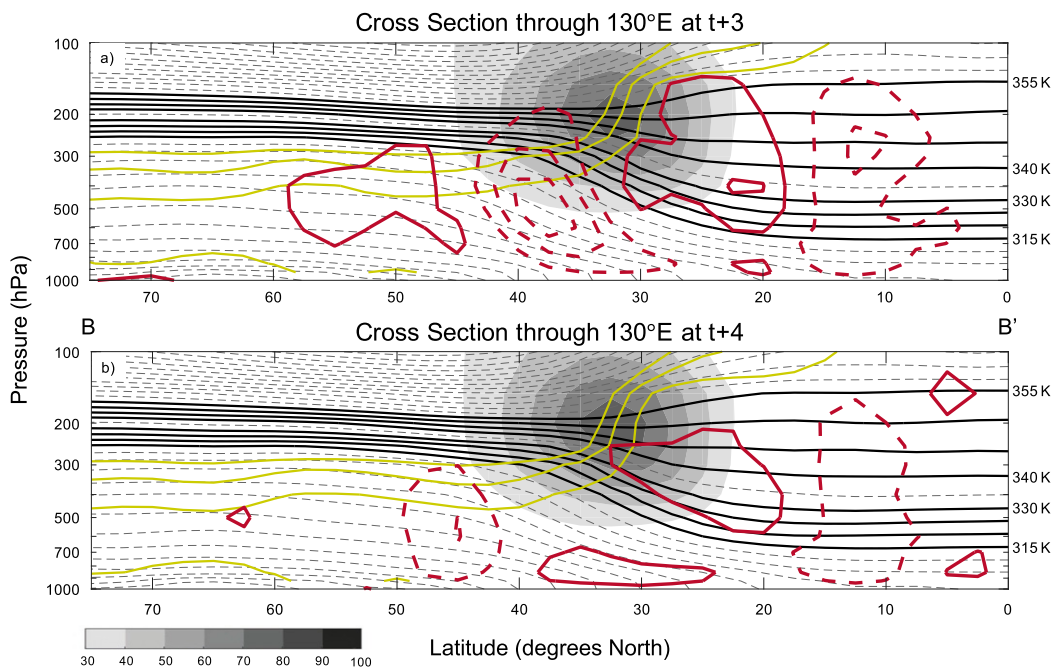


FIG. 15. As in Fig. 14, but at times (a) $t + 3$ and (b) $t + 4$ days.

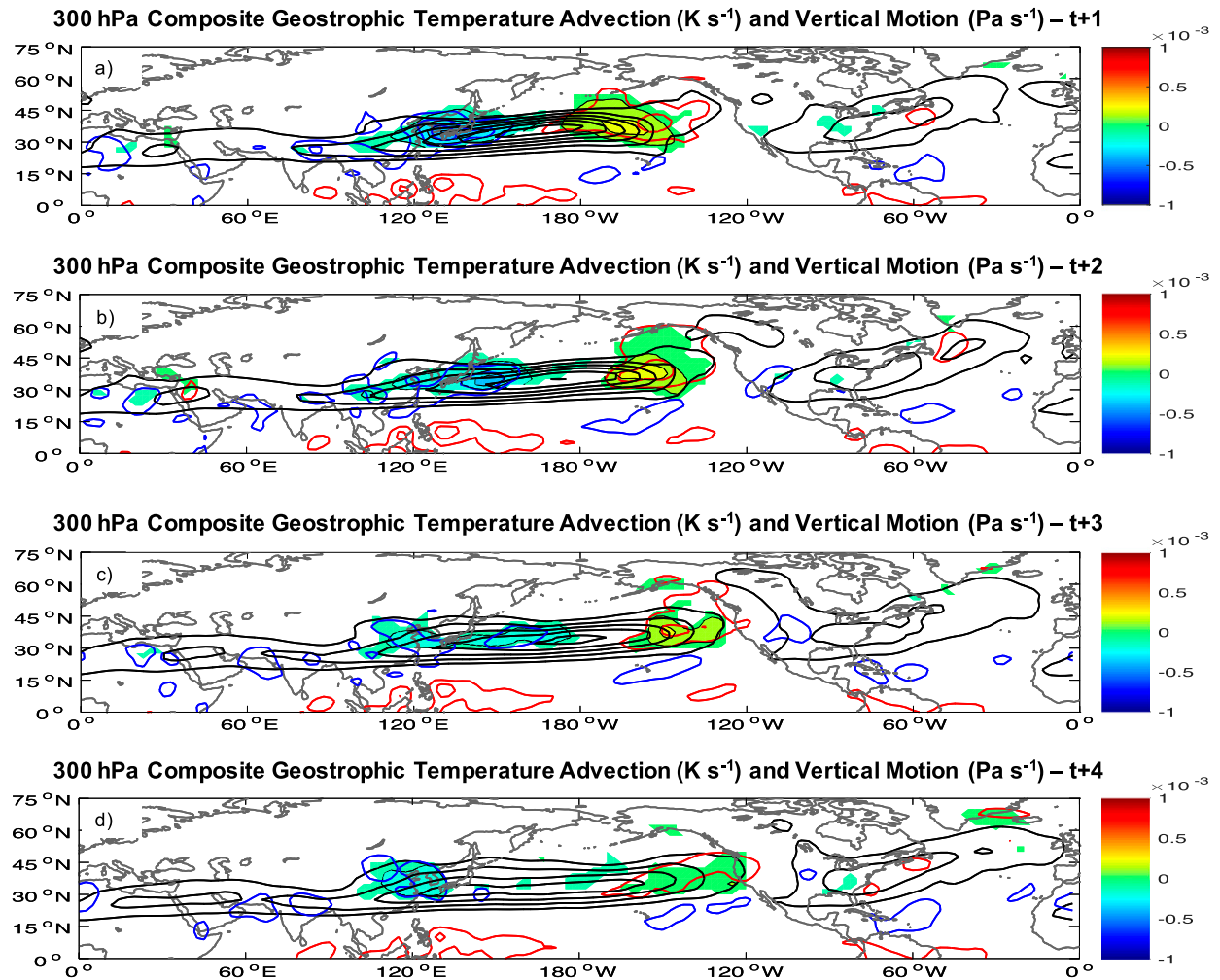


FIG. 16. The 300 hPa composite geostrophic temperature advection (fill pattern; K s^{-1}) and vertical motion (red contours indicate upward vertical motion, and blue contours indicate downward vertical motion) contoured every 0.05 Pa s^{-1} starting at $\pm 0.05 \text{ Pa s}^{-1}$ for times (a) $t + 1$, (b) $t + 2$, (c) $t + 3$, and (d) $t + 4$ days. Also plotted in all panels is the 300 hPa composite wind speed (black solid contours) every 10 m s^{-1} starting at 30 m s^{-1} .

to maximum poleward shift of the jet. This suggests that cold-surge events and associated anomalous convection at lower latitudes serve as precursor events associated with subsequent west Pacific jet extension/poleward shift. In summary, the results from this study, in concert with findings from Jaffe et al. (2011), Handlos and Martin (2016) and Griffin and Martin (2017), suggest that identification of jet-superposition events and their associated East Asian winter monsoon cold surges may offer predictive value regarding the evolution of the basin-wide large-scale circulation on synoptic time scales (i.e., 5–7 days).

5. Conclusions

The goal of this study was to explore the evolution of west Pacific vertical jet-superposition events and their associated large-scale environments in the days following initial superposition, extending the investigation of the pre-superposition

evolutions explored by Handlos and Martin (2016). This analysis, combined with the results shown in Handlos and Martin (2016), provide insight into the composite life cycle of jet-superposition events in the west Pacific, which has implications on the Northern Hemisphere large-scale circulation. The same composite and case-study analysis techniques used in Handlos and Martin (2016) were applied but at times after peak JSID. These evolutions were investigated within the context of the composite of 44 robust west Pacific vertical jet-superposition events.

Figure 18 highlights the key large-scale phenomena observed at the time of jet superposition (Fig. 18a; adapted from Fig. 17 of Handlos and Martin 2016) and after the time of jet superposition within the 44-case composite (Fig. 18b). West Pacific jet-superposition events are commonly associated with an East Asian winter monsoon northerly cold-surge event that propagates equatorward and enhances convection via enhanced surface convergence (dark blue oval with purple arrows

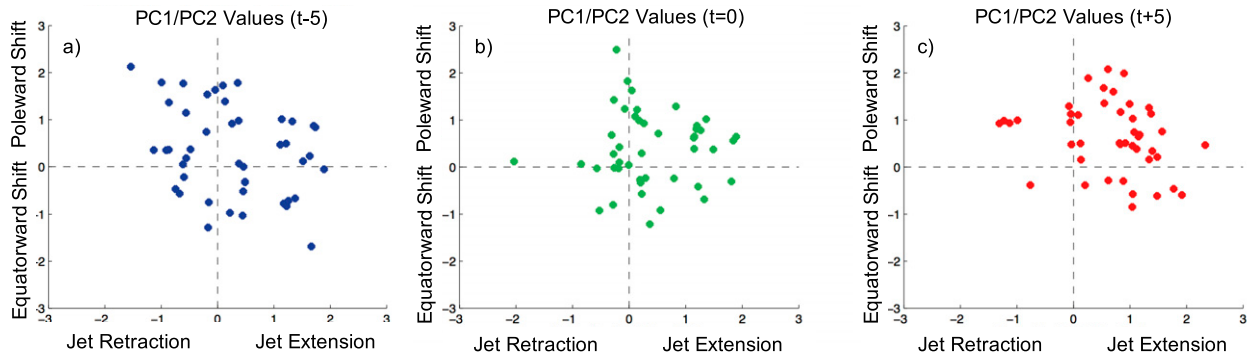


FIG. 17. (a) Phase space diagram showing values of normalized principal component (PC) modes 1 (i.e., jet extension and retraction) and 2 (i.e., poleward and equatorward shifts) for each of the 44 jet-superposition cases in this study at time $t - 5$ days. (b) As in (a), but for time $t = 0$. (c) As in (a), but for time $t + 5$ days. See text for further details.

interacting with cloud symbols in Fig. 18a). Low-PV air associated with the convective outflow (green stippled arrow) is then advected toward the anticyclonic shear side of the jet, increasing anomalous vertical wind shear such that the magnitude of wind within the jet core increases. This low-PV air, in concert with internal jet dynamics, also acts to develop the deep, vertical PV wall characteristic of west Pacific jet-superposition events.

In general, the evolution of the composite environments after superposition are all associated with the following: 1) the extension of the west Pacific jet stream; 2) the maintenance of anomalous cyclonic and anticyclonic flow in the left and right jet exit regions, respectively, that migrates eastward as the jet extends; 3) ridging downstream of the extended jet, which can lead to trough/ridge development downstream over eastern North America and the North Atlantic; 4) weakening of the East Asian winter monsoon northerly cold surge; and 5) the movement of upper-tropospheric anomalous southwesterly flow away from anomalous convection observed over the Maritime Continent region (Fig. 18b). Throughout this evolution, the west Pacific jet is displaced increasingly eastward from the environments that fostered superposition onset, perturbing the large-scale flow downstream and ultimately impacting the large-scale circulation over Alaska and northwestern Canada. Robust west Pacific vertical jet-superposition events last on average about 1–2 days. Consequently, the large-scale evolutions discussed in this paper and in Handlos and Martin (2016) are not by-products of jet superposition but instead work in concert to produce these jet-superposition events.

Examination of composite vertical cross sections through the composite jet core and entrance regions reveal the following: 1) weakening of the composite deep and vertical PV wall within the jet core and 2) a weakening of the thermally direct circulation within the composite jet entrance region. The first is tied to the eastward propagation of the positive and negative geopotential height anomalies flanking the jet core eastward within the jet exit regions and the subsequent weakening of southwesterly flow that advects low-PV air into the subtropical jet layer during jet-superposition development. The second is associated with the weakening of geostrophic cold-air advection along the axis of the composite jet entrance region.

The evolution of the composite life cycle of the west Pacific jet from time $t - 5$ to $t + 5$ days is somewhat represented using the two leading modes of jet variability extracted via PCA of 300 hPa zonal wind over the western Pacific. While significant variability is exhibited in PC1/PC2 evolution characterizing each individual case, the 44 cases exhibit an aggregate shift toward an extended/poleward-shifted jet. While recent research investigating the evolution of the west Pacific jet using PC modes 1 and 2 shows that PC1 and PC2 provide value in predicting the evolution of the west Pacific jet (e.g., Winters et al. 2019b), this study shows that these PCs do not exhibit robust predictability with respect to west Pacific jet-superposition events given the significant variability observed between the 44 individual cases investigated.

With recent research showing that extreme weather events can be influenced by vertical jet-superposition events (e.g., Christenson and Martin 2012; Winters and Martin 2014, 2016), it is reasonable to consider the effect of west Pacific vertical jet-superposition events on extreme weather over the Northern Hemisphere. For example, Archambault et al. (2007, 2013) show that recurving tropical cyclones in the west Pacific induce advection of low-PV outflow by the irrotational wind toward the jet entrance region of the west Pacific jet. This, in turn, induces a jet response that can lead to jet strengthening as well as a change in the large-scale flow over the Pacific Ocean and North America. These responses can lead to development of events such as strong extratropical cyclone development near Alaska, the development of a western North American anticyclonic “blocking” event and extreme temperature events over the United States (e.g., see Winters et al. 2019a, regarding the relationship between the North Pacific jet and extreme temperature events in the United States). Motivated by this, future work will explore the role tropical cyclones play in influencing west Pacific vertical jet-superposition development as well as the relationship between jet superpositions in this region and frequency of occurrence of blocking events and extreme temperature and precipitation events over North America.

Along with investigation of the above topics within future work, more detailed investigation of the specific synoptic-scale evolutions themselves post-superposition will help improve

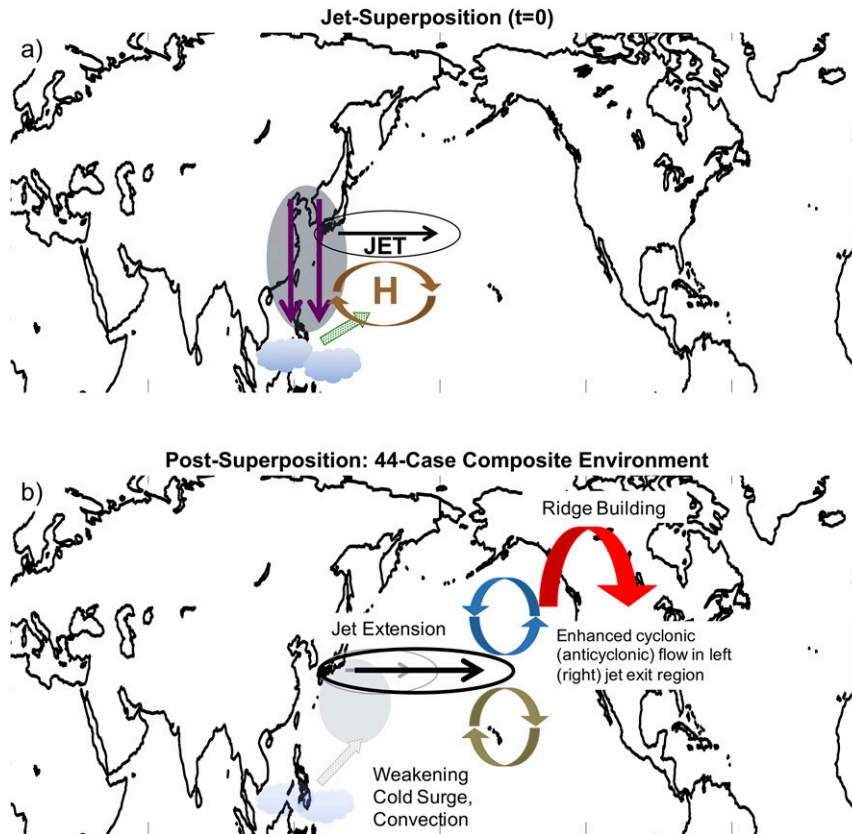


FIG. 18. Conceptual model highlighting evolution of the west Pacific jet and associated large-scale environments after time of west Pacific vertical jet-superposition occurrence. (a) Key large-scale components associated with west Pacific jet superposition [same conventions as that of Fig. 17 from Handlos and Martin (2016)] at time $t = 0$. (b) As in (a), but 1–4 days after superposition occurrence. The features shown in this panel are those that occur within the majority of cases within the 44-case composite. The jet extension that occurs during this time frame is shown as a black solid contour with a black vector; the jet at time $t = 0$ is shown as a light gray contour with a gray vector. The cyclonic (anticyclonic) circulation in teal (gold) represents the anomalous negative (positive) ϕ within the left (right) jet exit region that propagates eastward as the west Pacific jet extends. The red arrow over northwestern Canada represents the ridge that develops associated with anomalous positive ϕ at 250 and 500 hPa. This ridge develops as the jet extends eastward along with the anomalous cyclonic (anticyclonic) feature in the left (right) jet exit region. Finally, features that were significant in the 44-case composite environment at time $t = 0$ but have weakened at times $t + 1$ through $t + 4$ days are faded, including the weakening of the northerly cold-surge event.

understanding of the downstream large-scale circulation response to west Pacific vertical jet-superposition events. For example, the observed anomalous ridging in the east Pacific within the composite analysis may be the result of east Pacific Rossby wave breaking. However, this may not be true within all cases included within the composite analysis when investigated individually. Future work will require creation of jet-superposition subcategories to better understand the variability in downstream large-scale evolutions that result from these superposition events.

Acknowledgments. This work is funded by the National Science Foundation through Grant ATM-1265182.

Data availability statement. The authors of this study used the NCEP–NCAR Reanalysis I dataset Kalnay et al. (1996). Data files were acquired from the NCAR/UCAR Data Research Archive (<https://rda.ucar.edu/>).

REFERENCES

- Anderson, J. D., and R. D. Rosen, 1983: The latitude–height structure of 40–50 day variations in atmospheric angular momentum. *J. Atmos. Sci.*, **40**, 1584–1591, [https://doi.org/10.1175/1520-0469\(1983\)040<1584:TLHSOD>2.0.CO;2](https://doi.org/10.1175/1520-0469(1983)040<1584:TLHSOD>2.0.CO;2).
- Archambault, H. M., L. F. Bosart, and D. Keyser, 2007: Recurring typhoons as precursors to an early season Arctic outbreak over the continental U.S. *Ninth Northeast Regional*

- Operational Workshop*, Albany, NY, National Weather Service/Amer. Meteor. Soc., 1–55, <http://cstar.cestm.albany.edu/nrow/nrow9/Archambault/archambault.ppt>.
- , —, —, and J. M. Cordiera, 2013: A climatological analysis of the extratropical flow response to recurving western North Pacific tropical cyclones. *Mon. Wea. Rev.*, **141**, 2325–2346, <https://doi.org/10.1175/MWR-D-12-00257.1>.
- Athanasiadis, P. J., J. M. Wallace, and J. J. Wettstein, 2010: Patterns of wintertime jet stream variability and their relation to storm tracks. *J. Atmos. Sci.*, **67**, 1361–1381, <https://doi.org/10.1175/2009JAS3270.1>.
- Boyle, J. S., and T.-J. Chen, 1987: Synoptic aspects of the wintertime east Asian monsoon. *Monsoon Meteorology*, C.-P. Chang and T. N. Krishnamurti, Eds., Oxford University Press, 125–160.
- Chan, J. C. L., and C. Y. Li, 2004: The East Asian winter monsoon. *The Asian Monsoon*, C. Chang, Ed., World Scientific, 54–106.
- Chang, C.-P., and K.-M. Lau, 1980: Northeasterly cold surges and near-equatorial disturbances over the winter MONEX area during 1974. Part II: Planetary-scale aspects. *Mon. Wea. Rev.*, **108**, 298–312, [https://doi.org/10.1175/1520-0493\(1980\)108<0298:NCSANE>2.0.CO;2](https://doi.org/10.1175/1520-0493(1980)108<0298:NCSANE>2.0.CO;2).
- , J. Erickson, and K.-M. Lau, 1979: Northeasterly cold surges and near-equatorial disturbances over the winter MONEX area during 1974. Part I: Synoptic aspects. *Mon. Wea. Rev.*, **107**, 812–829, [https://doi.org/10.1175/1520-0493\(1979\)107<0812:NCSANE>2.0.CO;2](https://doi.org/10.1175/1520-0493(1979)107<0812:NCSANE>2.0.CO;2).
- , J. E. Millard, and G. T. J. Chen, 1983: Gravitational character of cold surges during winter MONEX. *Mon. Wea. Rev.*, **111**, 293–307, [https://doi.org/10.1175/1520-0493\(1983\)111<0293:GCOCSO>2.0.CO;2](https://doi.org/10.1175/1520-0493(1983)111<0293:GCOCSO>2.0.CO;2).
- , P. A. Harr, and H.-J. Chen, 2005: Synoptic disturbances over the equatorial South China Sea and western maritime continent during boreal winter. *Mon. Wea. Rev.*, **133**, 489–503, <https://doi.org/10.1175/MWR-2868.1>.
- Chin, P., 1969: Cold surges over South China. Royal Observatory Hong Kong Tech. Rep. 28, 40 pp.
- Christenson, C. E., and J. E. Martin, 2012: The large-scale environment associated with the 25–28 April 2011 severe weather outbreak. *16th Annual Severe Storms and Doppler Radar Conf.*, Des Moines, IA, National Weather Association.
- , —, and Z. J. Handlos, 2017: A synoptic climatology of Northern Hemisphere, cold season polar and subtropical jet superposition events. *J. Climate*, **30**, 7231–7246, <https://doi.org/10.1175/JCLI-D-16-0565.1>.
- Chu, P. S., A. J. Nash, and F. Y. Porter, 1993: Diagnostic studies of two contrasting rainfall episodes in Hawaii: Dry 1981 and wet 1982. *J. Climate*, **6**, 1457–1462, [https://doi.org/10.1175/1520-0442\(1993\)006<1457:DSOTCR>2.0.CO;2](https://doi.org/10.1175/1520-0442(1993)006<1457:DSOTCR>2.0.CO;2).
- Cunningham, P., and D. Keyser, 2004: Dynamics of jet streaks in a stratified quasi-geostrophic atmosphere: Steady-state representations. *Quart. J. Roy. Meteor. Soc.*, **130**, 1579–1609, <https://doi.org/10.1256/qj.03.35>.
- Davies, H., and A. Rossa, 1998: PV frontogenesis and upper tropospheric fronts. *Mon. Wea. Rev.*, **126**, 1528–1539, [https://doi.org/10.1175/1520-0493\(1998\)126<1528:PFAUTF>2.0.CO;2](https://doi.org/10.1175/1520-0493(1998)126<1528:PFAUTF>2.0.CO;2).
- Defant, F., and H. Taba, 1957: The threefold structure of the atmosphere and the characteristics of the tropopause. *Tellus*, **9**, 259–274, <https://doi.org/10.3402/tellusa.v9i3.9112>.
- Delcambre, S. C., D. J. Lorenz, D. J. Vimont, and J. E. Martin, 2013: Diagnosing Northern Hemisphere jet portrayal in 17 CMIP3 global climate models: Twentieth-century intermodel variability. *J. Climate*, **26**, 4910–4929, <https://doi.org/10.1175/JCLI-D-12-00337.1>.
- Griffin, K. S., and J. E. Martin, 2017: Synoptic features associated with temporally coherent modes of variability of the North Pacific jet stream. *J. Climate*, **30**, 39–54, <https://doi.org/10.1175/JCLI-D-15-0833.1>.
- Handlos, Z. J., and J. E. Martin, 2016: Composite analysis of large-scale environments conducive to West Pacific polar/subtropical jet superposition. *J. Climate*, **29**, 7145–7165, <https://doi.org/10.1175/JCLI-D-16-0044.1>.
- Held, I., 1975: Momentum transport by quasi-geostrophic eddies. *J. Atmos. Sci.*, **32**, 1494–1497, [https://doi.org/10.1175/1520-0469\(1975\)032<1494:MTBQGE>2.0.CO;2](https://doi.org/10.1175/1520-0469(1975)032<1494:MTBQGE>2.0.CO;2).
- Jaffe, S. C., J. E. Martin, D. J. Vimont, and D. J. Lorenz, 2011: A synoptic-climatology of episodic, subseasonal retractions of the Pacific jet. *J. Climate*, **24**, 2846–2860, <https://doi.org/10.1175/2010JCLI3995.1>.
- Johnson, R. H., and D. L. Priegnitz, 1981: Winter monsoon convection in the vicinity of North Borneo. Part II: Effects on large-scale fields. *Mon. Wea. Rev.*, **109**, 1615–1628, [https://doi.org/10.1175/1520-0493\(1981\)109<1615:WMCITV>2.0.CO;2](https://doi.org/10.1175/1520-0493(1981)109<1615:WMCITV>2.0.CO;2).
- Kalnay, E., and Coauthors, 1996: The NCEP/NCAR 40-Year Reanalysis Project. *Bull. Amer. Meteor. Soc.*, **77**, 437–471, [https://doi.org/10.1175/1520-0477\(1996\)077<0437:TNYRP>2.0.CO;2](https://doi.org/10.1175/1520-0477(1996)077<0437:TNYRP>2.0.CO;2).
- Kelnosky, R. T., G. J. Tripoli, and J. E. Martin, 2018: Subtropical/polar jet influence on plains and southeast tornado outbreaks. *Nat. Hazards*, **93**, 373–392, <https://doi.org/10.1007/s11069-018-3306-z>.
- Keyser, D., and M. A. Shapiro, 1986: A review of the structure and dynamics of upper-level frontal zones. *Mon. Wea. Rev.*, **114**, 452–499, [https://doi.org/10.1175/1520-0493\(1986\)114<0452:AROTSA>2.0.CO;2](https://doi.org/10.1175/1520-0493(1986)114<0452:AROTSA>2.0.CO;2).
- Knutson, T. R., and K. M. Weickmann, 1987: 30–60 day atmospheric oscillations: Composite life cycles of convection and circulation anomalies. *Mon. Wea. Rev.*, **115**, 1407–1436, [https://doi.org/10.1175/1520-0493\(1987\)115<1407:DAOCLC>2.0.CO;2](https://doi.org/10.1175/1520-0493(1987)115<1407:DAOCLC>2.0.CO;2).
- Kodama, K., and G. M. Barnes, 1997: Heavy rain events over the south-facing slopes of Hawaii: Attendant conditions. *Wea. Forecasting*, **12**, 347–367, [https://doi.org/10.1175/1520-0434\(1997\)012<0347:HREOTS>2.0.CO;2](https://doi.org/10.1175/1520-0434(1997)012<0347:HREOTS>2.0.CO;2).
- Koteswaram, P., 1953: An analysis of the high tropospheric wind circulation over India in winter. *Indian J. Meteor. Geophys.*, **4**, 13–21.
- , and S. Parthasarathy, 1954: The mean jet stream over India in the pre-monsoon and post-monsoon seasons and vertical motions associated with subtropical jet streams. *Indian J. Meteor. Geophys.*, **5**, 138–156.
- Krishnamurti, T. N., 1961: On the role of the subtropical jet stream of winter in the atmospheric general circulation. *J. Meteor.*, **18**, 657–670, [https://doi.org/10.1175/1520-0469\(1961\)018<0657:OTROTS>2.0.CO;2](https://doi.org/10.1175/1520-0469(1961)018<0657:OTROTS>2.0.CO;2).
- Kushnir, Y., and J. M. Wallace, 1989: Low-frequency variability in the Northern Hemisphere winter: Geographical distribution, structure and time-scale dependence. *J. Atmos. Sci.*, **46**, 3122–3143, [https://doi.org/10.1175/1520-0469\(1989\)046<3122:LFVITN>2.0.CO;2](https://doi.org/10.1175/1520-0469(1989)046<3122:LFVITN>2.0.CO;2).
- Lau, K.-M., and T. J. Phillips, 1986: Coherent fluctuations of extratropical geopotential height and tropical convection in intraseasonal timescales. *J. Atmos. Sci.*, **43**, 1164–1181, [https://doi.org/10.1175/1520-0469\(1986\)043<1164:CFOFGH>2.0.CO;2](https://doi.org/10.1175/1520-0469(1986)043<1164:CFOFGH>2.0.CO;2).
- , and C.-P. Chang, 1987: Planetary scale aspects of winter monsoon and teleconnections. *Monsoon Meteorology*, C.-P. Chang and T. N. Krishnamurti, Eds., Oxford University Press, 161–202.
- Liebmann, B., and D. L. Hartmann, 1984: An observational study of tropical-midlatitude interaction on intraseasonal time-scales during winter. *J. Atmos. Sci.*, **41**, 3333–3350, [https://doi.org/10.1175/1520-0469\(1984\)041<3333:AOSOTI>2.0.CO;2](https://doi.org/10.1175/1520-0469(1984)041<3333:AOSOTI>2.0.CO;2).

- Livezey, R. E., and K. C. Mo, 1987: Tropical–extratropical teleconnections during Northern Hemisphere winter. Part II: Relationships between monthly mean Northern Hemisphere circulations patterns and proxies for tropical convection. *Mon. Wea. Rev.*, **115**, 3115–3132, [https://doi.org/10.1175/1520-0493\(1987\)115<3115:TETDTN>2.0.CO;2](https://doi.org/10.1175/1520-0493(1987)115<3115:TETDTN>2.0.CO;2).
- Loewe, F., and V. Radok, 1950a: A meridional aerological cross section in the southwest Pacific. *J. Meteor.*, **7**, 58–65, [https://doi.org/10.1175/1520-0469\(1950\)007<0058:AMACSI>2.0.CO;2](https://doi.org/10.1175/1520-0469(1950)007<0058:AMACSI>2.0.CO;2).
- , and —, 1950b: Some amendments to “A meridional aerological cross-section in the southwest Pacific.” *J. Meteor.*, **7**, 305–306, [https://doi.org/10.1175/1520-0469\(1950\)007<0306:SATAMA>2.0.CO;2](https://doi.org/10.1175/1520-0469(1950)007<0306:SATAMA>2.0.CO;2).
- Martin, J. E., 2012: *Introduction to Weather and Climate Science*. Cognella Publishing, 153 pp.
- Matthews, A. J., and G. N. Kiladis, 1999: The tropical–extratropical interaction between high-frequency transients and the Madden–Julian oscillation. *Mon. Wea. Rev.*, **127**, 661–677, [https://doi.org/10.1175/1520-0493\(1999\)127<0661:TTEIBH>2.0.CO;2](https://doi.org/10.1175/1520-0493(1999)127<0661:TTEIBH>2.0.CO;2).
- McWilliams, J., and J. Chow, 1981: Equilibrium geostrophic turbulence. I: A reference solution in a β -plane channel. *J. Phys. Oceanogr.*, **11**, 921–949, [https://doi.org/10.1175/1520-0485\(1981\)011<0921:EGTIAR>2.0.CO;2](https://doi.org/10.1175/1520-0485(1981)011<0921:EGTIAR>2.0.CO;2).
- Mo, K., and V. E. Kousky, 1993: Further analysis of the relationship between circulation anomaly patterns and tropical convection. *J. Geophys. Res.*, **98**, 5103–5113, <https://doi.org/10.1029/92JD02952>.
- Mohri, K., 1953: On the fields of wind and temperature over Japan and adjacent waters during winter of 1950–1951. *Tellus*, **5**, 340–358, <https://doi.org/10.3402/tellusa.v5i3.8582>.
- Moore, R. W., O. Martius, and T. Spengler, 2010: The modulation of the subtropical and extratropical atmosphere in the Pacific basin in response to the Madden–Julian oscillation. *Mon. Wea. Rev.*, **138**, 2761–2779, <https://doi.org/10.1175/2010MWR3194.1>.
- Morrice, A. M., 1973: Quantitative forecasting of the winter monsoon in Hong Kong. Royal Observatory Hong Kong Tech. Rep. 35, 41 pp.
- Namias, J., and P. F. Clapp, 1949: Confluence theory of the high tropospheric jet stream. *J. Meteor.*, **6**, 330–336, [https://doi.org/10.1175/1520-0469\(1949\)006<0330:CTOTHT>2.0.CO;2](https://doi.org/10.1175/1520-0469(1949)006<0330:CTOTHT>2.0.CO;2).
- Newton, C. W., 1954: Frontogenesis and frontolysis as a three-dimensional process. *J. Meteor.*, **11**, 449–461, [https://doi.org/10.1175/1520-0469\(1954\)011<0449:FafaAT>2.0.CO;2](https://doi.org/10.1175/1520-0469(1954)011<0449:FafaAT>2.0.CO;2).
- Otkin, J. A., and J. E. Martin, 2004: The large-scale modulation of subtropical cyclogenesis in the central and eastern Pacific Ocean. *Mon. Wea. Rev.*, **132**, 1813–1828, [https://doi.org/10.1175/1520-0493\(2004\)132<1813:TLMOsc>2.0.CO;2](https://doi.org/10.1175/1520-0493(2004)132<1813:TLMOsc>2.0.CO;2).
- Palmén, E., and C. W. Newton, 1969: *Atmospheric Circulation Systems: Their Structure and Physical Interpretation*. Academic Press, 603 pp.
- Panetta, R., 1993: Zonal jets in wide baroclinically unstable regions: Persistence and scale selection. *J. Atmos. Sci.*, **50**, 2073–2106, [https://doi.org/10.1175/1520-0469\(1993\)050<2073:ZJIWBU>2.0.CO;2](https://doi.org/10.1175/1520-0469(1993)050<2073:ZJIWBU>2.0.CO;2).
- Reiter, E. R., 1963: *Jet Stream Meteorology*. University of Chicago Press, 515 pp.
- Rhines, P., 1975: Waves and turbulence on a β -plane. *J. Fluid Mech.*, **69**, 417–443, <https://doi.org/10.1017/S0022112075001504>.
- Riehl, H., 1962: Jet streams of the atmosphere. Department of Atmospheric Science, Colorado State University Tech. Rep. 32, 117 pp.
- Sardeshmukh, P. D., and B. J. Hoskins, 1988: The generation of global rotational flow by steady idealized tropical divergence. *Mon. Wea. Rev.*, **45**, 1228–1251, [https://doi.org/10.1175/1520-0469\(1988\)045<1228:TGOGRF>2.0.CO;2](https://doi.org/10.1175/1520-0469(1988)045<1228:TGOGRF>2.0.CO;2).
- Schubert, S. D., and C.-K. Park, 1991: Low frequency intra-seasonal tropical–extratropical interactions. *J. Atmos. Sci.*, **48**, 629–650, [https://doi.org/10.1175/1520-0469\(1991\)048<0629:LFITEI>2.0.CO;2](https://doi.org/10.1175/1520-0469(1991)048<0629:LFITEI>2.0.CO;2).
- Shapiro, M., and D. Keyser, 1990: Fronts, jet streams, and the tropopause. *Extratropical Cyclones: The Erik Palmén Memorial Volume*, C. Newton and E. O. Holopainen, Eds., Amer. Meteor. Soc., 167–191.
- , and Coauthors, 1999: A planetary-scale to mesoscale perspective of the life cycles of extratropical cyclones: The bridge between theory and observations. *The Life Cycles of Extratropical Cyclones*, M. A. Shapiro and S. Grønås, Eds., Amer. Meteor. Soc., 139–185.
- Sutcliffe, R. C., and J. K. Bannon, 1954: Seasonal changes in the upper-air conditions in the Mediterranean Middle East area. *Scientific Proc. Int. Association of Meteorology*, Rome, Italy, International Union of Geodesy and Geophysics, 322–334.
- Wang, L., and W. Chen, 2014: An intensity index for the East Asian winter monsoon. *J. Climate*, **27**, 2361–2374, <https://doi.org/10.1175/JCLI-D-13-00086.1>.
- Weickmann, K. M., G. R. Lussky, and J. E. Kutzbach, 1985: Intraseasonal (30–60 day) fluctuations of outgoing longwave radiation and 250 mb streamfunction during northern winter. *Mon. Wea. Rev.*, **113**, 941–961, [https://doi.org/10.1175/1520-0493\(1985\)113<0941:IDFOOL>2.0.CO;2](https://doi.org/10.1175/1520-0493(1985)113<0941:IDFOOL>2.0.CO;2).
- Winters, A. C., and J. E. Martin, 2014: The role of a polar/subtropical jet superposition in the May 2010 Nashville flood. *Wea. Forecasting*, **29**, 954–974, <https://doi.org/10.1175/WAF-D-13-00124.1>.
- , and —, 2016: Synoptic and mesoscale processes supporting vertical superposition of the polar and subtropical jets in two contrasting cases. *Quart. J. Roy. Meteor. Soc.*, **142**, 1133–1149, <https://doi.org/10.1002/qj.2718>.
- , and —, 2017: Diagnosis of a North American polar–subtropical jet superposition employing piecewise potential vorticity inversion. *Mon. Wea. Rev.*, **145**, 1853–1873, <https://doi.org/10.1175/MWR-D-16-0262.1>.
- , L. F. Bosart, and D. Keyser, 2019a: Antecedent North Pacific jet regimes conducive to the development of continental U.S. extreme temperature events during the cool season. *Wea. Forecasting*, **34**, 393–414, <https://doi.org/10.1175/WAF-D-18-0168.1>.
- , D. Keyser, and L. F. Bosart, 2019b: The development of the North Pacific jet phase diagram as an objective tool to monitor the state and forecast skill of the upper-tropospheric flow pattern. *Wea. Forecasting*, **34**, 199–219, <https://doi.org/10.1175/WAF-D-18-0106.1>.
- , —, —, and J. E. Martin, 2020: Composite synoptic-scale environments conducive to North American polar–subtropical jet superposition events. *Mon. Wea. Rev.*, **148**, 1987–2008, <https://doi.org/10.1175/MWR-D-19-0353.1>.
- Wu, M. C., and J. C. L. Chan, 1995: Surface features of winter monsoon surges over South China. *Mon. Wea. Rev.*, **123**, 662–680, [https://doi.org/10.1175/1520-0493\(1995\)123<0662:SFOVMS>2.0.CO;2](https://doi.org/10.1175/1520-0493(1995)123<0662:SFOVMS>2.0.CO;2).
- Yeh, T. C., 1950: The circulation of the high troposphere over China in the winter of 1945–46. *Tellus*, **2**, 173–183, <https://doi.org/10.3402/tellusa.v2i3.8548>.
- Zhang, Y., K. R. Sperber, and J. S. Boyle, 1997: Climatology and interannual variation of the East Asian winter monsoon: Results from the 1979–95 NCEP/NCAR reanalysis. *Mon. Wea. Rev.*, **125**, 2605–2619, [https://doi.org/10.1175/1520-0493\(1997\)125<2605:CAIVOT>2.0.CO;2](https://doi.org/10.1175/1520-0493(1997)125<2605:CAIVOT>2.0.CO;2).